

Software-Controlled Switch Reluctance Motors

ET15SCE1330



Prepared by:

*Emerging Products
Customer Service
Southern California Edison
August 2018*

Acknowledgments

Southern California Edison's (SCE) Emerging Products (EP) group is responsible for this project. It was developed as part of SCE's Emerging Technologies Program, under internal project number ET15SCE1330. Dallen Coulter conducted this technology evaluation with overall guidance and management from Jerine Ahmed. Western Cooling Efficiency Center (WCEC) was contracted to support this work, with significant contributions from Theresa Pistoichini and Caton Mande. For more information on this project, contact dallen.coulter@sce.com.

Disclaimer

This report was prepared by SCE and funded by California utility customers, under the auspices of the California Public Utilities Commission. Reproduction or distribution of the whole or any part of the contents of this document, without the express written permission of SCE, is prohibited. This work was performed with reasonable care and in accordance with professional standards. However, neither SCE nor any entity performing the work pursuant to SCE's authority make any warranty or representation, expressed or implied, with regard to this report, the merchantability or fitness for a particular purpose of the results of the work, or any analyses or conclusions contained in this report. The results reflected in the work are generally representative of operating conditions; however, the results in any other situation may vary, depending upon particular operating conditions.

Executive Summary

This project measured the performance of an emerging technology nominal three-horsepower (3HP) high rotor pole Switched Reluctance Motor (SRM) with software-controlled inverter, compared to a baseline nominal 3HP baseline induction motor controlled by a Variable-Frequency Drive (VFD) in laboratory testing, and a nominal 3HP baseline single-speed induction motor for field testing.

The difference in performance between the two motors was used to forecast annual energy and demand savings expected to result from replacing the baseline technology with the emerging technology.

Background

Packaged air conditioning and heating Roof Top Units (RTUs) provide an estimated 75% of the cooling to commercial buildings in California, and can account for more than 50% of peak electrical demand [1]. It has been documented that power savings are attainable by operating at lower fan speeds when possible [2] [3], primarily by reducing indoor fan speeds when RTUs are only providing ventilation or air circulation or during part load operation.

Variable indoor airflow is typically achieved by using a VFD that varies the indoor fan motor speed based on the RTU's operating mode. However, using a VFD to achieve variable speed control lowers the indoor blower system efficiency, which reduces the full savings potential.

Assessment Objectives

This project evaluated the potential of a high rotor pole SRM technology to save energy in Heating, Ventilation, and Air Conditioning (HVAC) systems. Power demand associated with indoor blower operation was reduced by increasing the air delivery system efficiency. This report describes the laboratory and field evaluation comparing the emerging technology nominal 3HP high rotor pole SRM with two 3HP induction motors:

Laboratory Evaluation:

- Baseline: Nominal 3HP three-phase induction motor with a VFD.
- Emerging Technology: Nominal 3HP high rotor pole SRM with a patented software-controlled inverter
- The laboratory technology evaluation included two components: 1) laboratory testing the motor systems on a benchtop dynamometer, and 2) laboratory testing the motor systems on a packaged 10-ton RTU.

Field Evaluation:

- Baseline: Nominal 3HP three-phase constant-speed induction motor
- Emerging Technology: Nominal 3HP high rotor pole SRM with a patented software-controlled inverter.
- The field evaluation included two phases: 1) operating the high rotor pole SRM at variable speeds based on the RTU mode; and 2) operating the high rotor pole SRM at a constant speed matching the Revolutions per Minute (RPM) of the baseline motor.

Laboratory Test Approach

Baseline and emerging technology performance was characterized using two different test setups: 1) a benchtop dynamometer; and 2) a laboratory RTU's indoor fan. For the benchtop dynamometer testing, each motor/drive was tested over seven different load conditions at six different speeds. For the laboratory RTU, each fan/motor/drive was tested over three fixed-resistance conditions at seven different fan speeds.

Laboratory Results

The benchtop dynamometer and laboratory RTU test results show the high rotor pole SRM with software-controlled inverter is a promising option for reducing fan power, when compared to an equivalent-sized induction motor.

In dynamometer testing, for the seven different load conditions, the high rotor pole SRM used 9.2% to 36.2% less power than the baseline induction motor and VFD system to generate the same torque. In laboratory RTU testing, the high rotor pole SRM reduced the fan power intensity, when retrofitted to the existing belt and fan configuration. On average, the high rotor pole SRM reduced the fan power intensity by 16.9%, 17.5%, and 21.3% for the low, medium, and high-airflow resistance conditions.

Field Testing Approach

Field testing was conducted between November 1, 2017 and August 31, 2018. A field site location in Corona, California was selected for testing, based on previous evaluations performed at that location. Over the test period, the 10-ton RTU was run with the baseline constant-speed fan, then retrofitted with the emerging technology high rotor pole SRM.

The retrofit motor was run in two modes: 1) a constant speed, matching the original baseline motor's rotational speed; and 2) variable speed, to demonstrate the additional energy savings possible by implementing a variable-speed blower control. Motor power, static pressure between the supply and return ducts, supply airflow, and supply and return air dry bulb and Relative Humidity (RH) were used to compare the performance of the baseline to the emerging technology.

Field Testing Results

During the field test, the baseline motor used 0.94 – 1.21 kilowatts (kW) while operating at 1,725 RPM. At the same operating speed, the high rotor pole SRM used 0.617 – 1.083 kW. On average, it reduced the required power draw by 15% compared to the baseline, and was able to obtain these savings with a power intensity that was, on average, 11.2% lower than the baseline motor.

Operating at variable speed achieved additional savings by reducing the airflow rate when full airflow was not required. During the variable-speed portion of the field test, the high rotor pole SRM used 0.855 kW while operating at 1,294 RPM (75% of full speed) for Stage 1 cooling, and 0.131 kW while operating at 690 RPM (40% of full speed) for air circulation.

Annualized Savings for SCE Service Territory

The potential annualized savings for the 3HP high rotor pole SRM was calculated for a 10-ton RTU with a centrifugal indoor fan (15" in diameter and 15" deep) that conditions a commercial space in SCE's service territory.

Annual energy usage was calculated based on the laboratory RTU and field testing results, the assumption the commercial space was open year-round for 14 hours per day with the RTU fan running, and the estimated number of hours annually (2371 hours) the RTU would operate in cooling or heating mode, based on the California End-Use Survey data [1]. The results illustrate the high rotor pole SRM could reduce annual energy usage by 50% to 57% when compared to the baseline single-speed induction motor, and 11% compared to an induction motor controlled by a VFD.

Recommendations

Based on the study results, high rotor pole SRMs with software-controlled inverters have the potential to save energy and reduce demand compared to constant-speed induction motors, as well as induction motors controlled by VFDs in RTU indoor fan applications. The savings was achieved through technological differences that allow the high rotor pole SRMs to operate at a higher efficiency over a range of load and speed conditions.

Abbreviations

AC	Alternating Current
ACFM	Actual Cubic Foot per Minute
CFM	Cubic Foot per Minute
DC	Direct Current
ESP	External Static Pressure
FTP	File Transfer Protocol
HP	Horsepower
HVAC	Heating, Ventilation, and Air Conditioning
HZ	Hertz
kW	Kilowatt
kWh	Kilowatt-hour
MSAV	Multi-Stage Air Volume
NEMA	National Electrical Manufacturers Association
RA	Return Air
RH	Relative Humidity
RMS	Root Mean Squared
RPM	Revolutions per Minute
RTU	Roof Top Unit
SA	Supply Air
SCE	Southern California Edison
SCFM	Standard Cubic Foot Per Minute
SRM	Switched Reluctance Motor
T	Air Temperature
TEFC	Totally Enclosed Fan Cooled
VFD	Variable-Frequency Drive

Contents

Executive Summary	i
Background.....	i
Assessment Objectives	i
Laboratory Test Approach.....	ii
Laboratory Results.....	ii
Field Testing Approach	ii
Field Testing Results	ii
Annualized Savings for SCE Service Territory	iii
Recommendations	iii
Abbreviations	iv
Contents	v
Figures	viii
Tables	ix
Equations	xi
Introduction	1
Background	1
Baseline Technology.....	3
Emerging Technology	4
Assessment Objectives	6
Technical Approach – Test Equipment	7
Baseline Equipment – Laboratory Testing.....	7
Baseline Equipment – Field Testing.....	8
Emerging Technology Equipment – Laboratory and Field Testing.....	8
Technical Approach – Laboratory Testing	9
Test Facility	9
Laboratory Benchtop Testing	10
Benchtop Dynamometer Overview	10
Benchtop Dynamometer Instrumentation	10
Benchtop Dynamometer Test Procedures	11

Laboratory RTU Testing	11
Laboratory RTU Overview	11
Laboratory RTU Instrumentation	13
Air Temperature and Relative Humidity Measurements	14
Differential Pressure Measurements	14
Airflow Measurements	14
Motor Speed	14
Power Measurements	15
Data Acquisition System	15
Laboratory RTU Test Procedures	15
Equations and Error Analysis	16
Benchtop Dynamometer Testing	16
Laboratory RTU Testing	17
Measurement Uncertainty	19
Results – Laboratory Testing	20
Benchtop Dynamometer Testing	20
Motor/Drive Efficiency	20
Torque versus Power	20
Power Factor	20
Combined Fan/Motor/Drive Efficiency	27
Fan Power Intensity	29
Uncertainty	30
Summary – Laboratory Testing	31
Technical Approach – Field Testing	32
Site and Unit Selection	32
Field Testing Overview	32
Instrumentation	33
Air Temperature and Relative Humidity Measurements	34
One-Time Tracer Gas Airflow Map Measurement	34
Differential Pressure Measurement	34
Power Measurement	34
Data Acquisition System	35
Equations and Error Analysis	35
Measurement Uncertainty	36

Results – Field Testing _____ **37**

 Airflow 37

 Fan Power Intensity..... 38

 Airflow vs Power..... 40

 Uncertainty..... 42

 Summary – Field Testing 42

Annualized Savings for SCE Service Territory _____ **43**

Conclusion _____ **45**

Recommendations _____ **45**

References _____ **46**

Figures

Figure 1: Induction (left) and SRM (right) Primary Component Schematic	2
Figure 2: Simple Three-Phase, Two-Pole Induction Motor Diagram	4
Figure 3: 6/4 SRM Operation Diagram.....	5
Figure 4: Lab Facility Diagram (left), Dynamometer Setup South Face (top right), Lab RTU West Face (lower right)	9
Figure 5: Baseline Motor (left) Dynamometer Setup	10
Figure 6: Plenum-Duct Apparatus Layout (with instrumentation)	12
Figure 7: Flexible Neoprene-Coated Polyester Duct Layout (with instrumentation)	13
Figure 8: Laboratory RTU Instrumentation Layout Schematic	14
Figure 9: RTU Manual Measuring Belt Tension (image from [10])	15
Figure 10: Power vs. Motor/drive Efficiency for Benchtop Dynamometer Test with 2 nd -Order Polynomial Fit	21
Figure 11: Torque vs. Power for Benchtop Dynamometer Test with Linear Fit ..	23
Figure 12: Power vs. Motor/Drive Power Factor for Dynamometer Testing with 2 nd -Order Polynomial Fit	25
Figure 13: Airflow vs. Fan/Motor/Drive Efficiency for Lab RTU Test.....	27
Figure 14: Airflow vs. Power Intensity for Laboratory RTU Testing.....	29
Figure 15: Bird's Eye View of Field Test Site (orange square shows RTU 24 location)	32
Figure 16: Field Test Instrumentation Schematic	33
Figure 17: Results of One-Time Tracer Gas Airflow Map to Differential Pressure between Supply and Return Ducts.....	35
Figure 18: Hourly Average Airflow during Field Test	38
Figure 19: Field Test Fan Power Intensity Comparison.....	39
Figure 20: Fixed-Speed Fan Power Intensity Comparison	40
Figure 21: Airflow vs. Power	41

Tables

Table 1: Nameplate Data for Lab Test Baseline Induction Motor and VFD	7
Table 2: Nameplate Data for Field Test Baseline Induction Motor	8
Table 3: Nameplate Data for High Rotor Pole SRM	8
Table 4: Benchtop Measurements.....	10
Table 5: Benchtop Dynamometer Test Points	11
Table 6: Laboratory RTU Test Measurements	13
Table 7: RTU Test Points	16
Table 8: Baseline System Motor/Drive Efficiency Summary Table (efficiency at each condition)	22
Table 9: High Rotor Pole SRM System Motor/Drive Efficiency Summary Table (efficiency at each condition).....	22
Table 10: Baseline System Motor/Drive Power Summary Table (watts at each condition)	24
Table 11: High Rotor Pole SRM System Motor/Drive Power Summary Table (watts at each condition)	24
Table 12: Baseline System Motor/Drive Power Factor Summary Table (power factor at each condition)	26
Table 13: High Rotor Pole SRM System Motor/Drive Power Factor Summary Table (power factor at each condition)	26
Table 14: Baseline System Fan/Motor/Drive Efficiency Summary Table (efficiency at each condition).....	28
Table 15: High Rotor Pole SRM System Fan/Motor/Drive Efficiency Summary Table (efficiency at each condition).....	28
Table 16: Baseline System Power Intensity Summary Table	30
Table 17: High Rotor Pole SRM System Power Intensity Summary Table	30
Table 18: Uncertainties for Typical Values.....	30
Table 19: Field Test Phases	33
Table 20: Field Test Measurements.....	34
Table 21: Airflow Range Observed during Various Test Phases	37
Table 22: Average Fan Power Intensity Results.....	39
Table 23: Average Power during Field Test	41
Table 24: Uncertainty of Calculated Metrics	42
Table 25: Inputs for SCE Service Territory Annualized Energy Savings Forecast.....	44

Table 26: Results of SCE Service Territory Annualized Energy Savings
Forecast..... 44

Equations

Equation 1: Motor Output Power	16
Equation 2: Motor/Drive Efficiency	16
Equation 3: Tracer Gas Airflow Measurement Calculation	17
Equation 4: SCFM-to-ACFM Conversion	17
Equation 5: Total Pressure	18
Equation 6: Dynamic Pressure	18
Equation 7: Airflow Velocity	18
Equation 8: Fan Output Power	18
Equation 9: Fan/Motor/Drive Efficiency	18
Equation 10: Fan Power Intensity	18
Equation 11: Uncertainty Using Sequential Perturbation	19
Equation 12: Field Test Airflow Map.....	35

Introduction

This project evaluated the potential of a high rotor pole Switched Reluctance Motor (SRM) technology to save energy in HVAC systems. The high rotor pole SRM technology reduces power demand associated with indoor fan operation by increasing air delivery system efficiency. This report describes the laboratory and field evaluation comparing the emerging technology nominal 3HP high rotor pole SRM with two nominal 3HP induction motors.

Laboratory Evaluation:

- Baseline – Nominal 3HP three-phase induction motor with VFD.
- Emerging Technology – Nominal 3HP high rotor pole SRM with patented software-controlled inverter.

The laboratory evaluation had two components: 1) testing the motor systems on a benchtop dynamometer; and 2) testing the motor systems in a packaged RTU.

Field Evaluation:

- Baseline – Nominal 3HP three-phase constant-speed induction motor.
- Emerging Technology – Nominal 3HP high rotor pole SRM with patented software-controlled inverter.

The field evaluation had three phases: 1) measuring the baseline induction motor's performance; 2) running the high rotor pole SRM at a constant speed, matching the baseline motor's RPM; and 3) operating the high rotor pole SRM at variable speeds, based on the RTU operating mode.

Background

Packaged air conditioning and heating RTUs provide an estimated 75% of cooling to commercial buildings in California, and can account for more than 50% of peak electrical demand [1]. It has been documented that power savings are attainable by operating at lower fan speeds when possible [2] [3], primarily by reducing indoor fan speeds during times when RTUs are only providing ventilation. Additionally, it is becoming more common for manufacturers to offer variable indoor airflow as an option for RTUs. This is typically achieved by using VFDs that vary indoor fan motor speeds based on RTU operating mode.

A field study that recorded in-situ measurements from 215 RTUs on newly-constructed, small commercial buildings in California found the average RTU uses 180 watts to deliver 325 Cubic Foot per Minute (CFM) per ton of cooling at an average duct system pressure drop of 0.48 inches of water [4]. Fan affinity laws derived using the Buckingham Pi method show fan power is proportional to the cubic of fan shaft speed, and flow rate is proportional to fan shaft speed. Combining the field study data and fan affinity laws, a 50% reduction in fan speed could, ideally, result in an 87.5% reduction in power. However, using a VFD to achieve variable speed control lowers the indoor fan system efficiency, making it harder to achieve the full savings potential. The lower system efficiency is a result of operating the induction motor below its design point, as well as additional losses from adding a VFD to the indoor fan system [5].

Induction motors are one of the most common type of electric motor in use [6]. The primary components of induction motors are stators (stationary parts), rotors (rotating parts), and wire windings, which create electromagnetic poles (Figure 1). Induction motors have windings on both the stator and rotor (Figure 1, left), and run at fixed shaft speeds

based on the frequency of the alternating current (AC) power supplied to the motor, as well as the number of stator poles. The motor's torque output depends on the difference between the rotational speed of the magnetic field generated in the stator, and the rotor's physical rotational speed, which is called "slip."

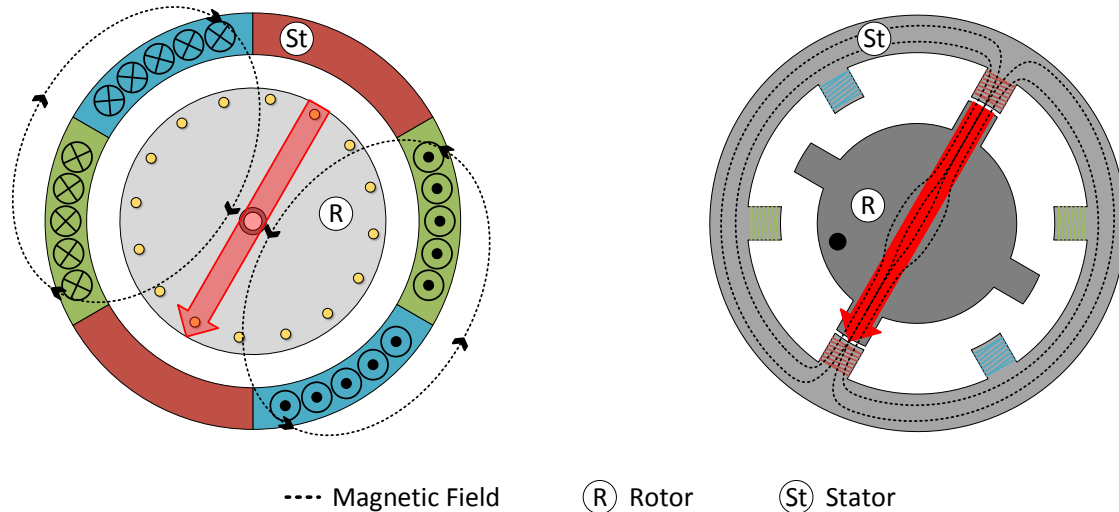


FIGURE 1: INDUCTION (LEFT) AND SRM (RIGHT) PRIMARY COMPONENT SCHEMATIC

SRMs are another variant of electrical motors and have been used in industrial applications since the 1850s. However, it wasn't until more recently, when cheap, reliable solid-state switching devices became available, that the technology's potential for wider use was realized [7]. High rotor pole SRMs are a subset of those that have non-traditional ratios of stator poles to rotor poles (i.e., 6/10 versus 6/4) [8]. Using non-traditional ratios reduces rotational travel per excitation, and increases static torque production [8] [9].

SRMs, in general, have the following differences compared to induction motors:

- The rotors are made of stacks of ferrous laminate material, and do not have windings (Figure 1, right).
- The stator poles are driven by direct current (DC) power, and require inverters when using AC power.

The stator winding current requires active control and cannot operate without an inverter/controller. For the high rotor pole SRM used in the study, the manufacturer's patented software-controlled inverter monitored the real-time motor parameters, and switched poles on and off to achieve the desired motor speed and torque.

Because high rotor pole SRM systems are actively controlled, they can operate at high efficiency over a range of operating conditions. Additionally, SRM inverters typically operate at higher efficiency compared to VFDs, since their switching frequencies are much slower.

The primary source of losses in inverters or VFDs comes from the energy required to operate their internal transistors. The losses are equal to the product of the frequency and the amount of power used to change transistor states. SRM switching frequency is dependent on the number of rotor poles and rotation speed. For example, a six-rotor pole SRM operating at 1,800 RPM has a 180HZ switching frequency. In contrast, a VFD relies on a high switching frequency, called the "carrier frequency," which is necessary to

approximate an AC voltage waveform. In laboratory testing, the VFD carrier frequency had a range of 0.7 – 14.5 kHz, which is between three and 80 times higher than the SRM switching frequency. Therefore, a high rotor pole SRM has the potential to reduce the energy and power demand associated with an RTU indoor fan by operating with high efficiency over a range of speeds.

Baseline Technology

The laboratory and field testing baseline technology included a three-phase induction motor controlled by a VFD, and a three-phase induction motor operating at a single speed.

In three-phase induction motors, stator windings are subjected to AC power supply phases, resulting in magnetic fields rotating around the axis of the motor shaft. The stator windings' rotating magnetic field create current in the rotor windings through induction, resulting in a rotor magnetic field that lag the stators. Interaction between the two magnetic fields generates force on the rotor.

Most induction motors are designed to run at fixed speeds based on three-phase AC power supply frequency. When variable speed operation is desired, VFDs are added to reduce voltage waveform frequency, which in turn reduces the stator's magnetic field rotational speed. This alters motor operation by slowing the rotor and changing the amount of torque produced.

Figure 2 illustrates a half revolution of a three-phase, two-pole (for simplification) induction motor and 60HZ voltage waveform. The stator is composed of six sections, with each color representing half of a stator coil. The coils are wound so the current flows in the opposite direction in each half. Current flowing in and out are denoted by circles with "Xs" and circles with dots, respectively. The ellipses represent a simplification of the magnetic field generated by the current, and the red arrows illustrate the resulting magnetic field orientation. The rotor is shown in gray, and the rotor coils are represented by the small yellow circles around the perimeter. The rotor makes a one-half rotation through the following four steps:

1. Current flows through the green and blue coils, orienting the magnetic field with the red coils.
2. When the current shifts to the red and blue coils, the magnetic field orientation shifts to the green coil.
3. When the current shifts to the red and green coils, the magnetic field orientation shifts to the blue coil.
4. The current returns to the green and blue coils, but flows in the opposite direction of (1), causing the magnetic field to orient with the red coils again, but with the North-South orientation switched.

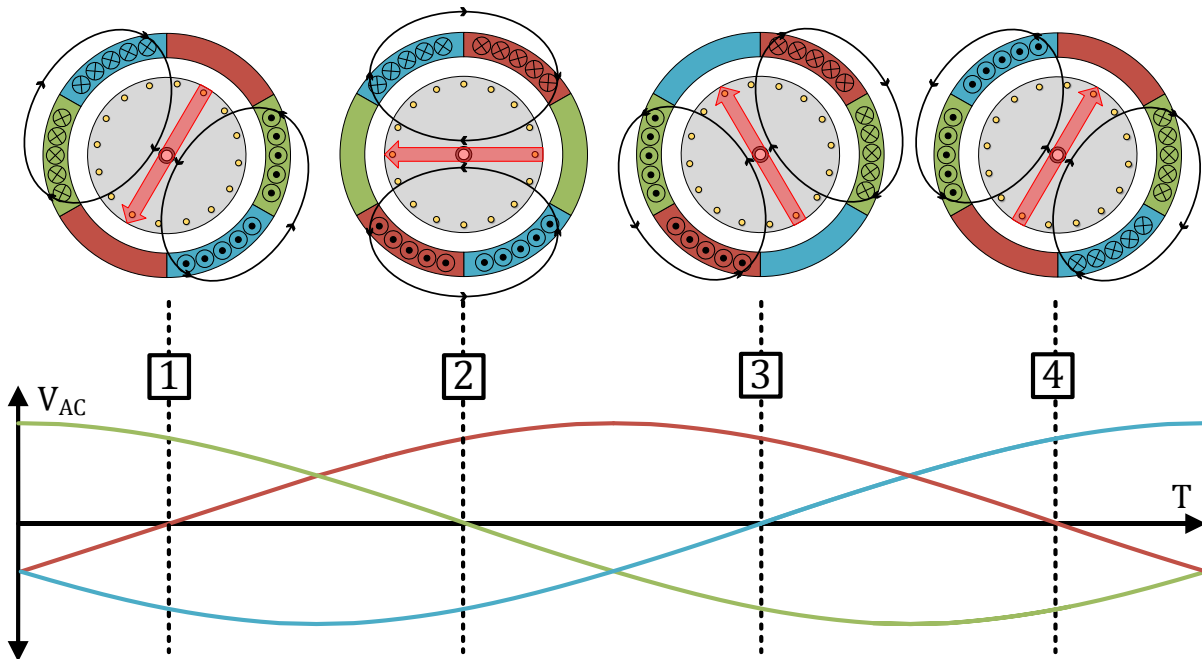


FIGURE 2: SIMPLE THREE-PHASE, TWO-POLE INDUCTION MOTOR DIAGRAM

Emerging Technology

An SRM operates on the principle of magnetic reluctance, which creates a force in the magnetic circuit toward the smallest magnetic resistance (also called “reluctance”). Because the rotor material has a lower reluctance than the air, the nearest rotor pole is pulled toward the energized stator coil, minimizing the magnetic reluctance. In an SRM, the stator windings are switched on and off (commutated) by the controller, to constantly pull the rotor toward the next activated winding, minimizing the magnetic reluctance and creating a torque around the motor shaft.

Figure 3 illustrates a half rotation of a simple SRM with six stator poles and four rotor poles. Each pair of stator poles is color coded (red, green, or blue). The rotor makes a one-half rotation through the following four steps (the black dot provides a rotor position reference point):

1. The red coil is energized, pulling the closest stator poles to align with it.
2. The blue stator coil is energized, pulling the closest pole (positioned clockwise from the reference dot) to align with the blue coil.
3. The green stator coil is energized, pulling the closest pole (positioned counter-clockwise from the reference dot) to align with the green coil.
4. The red stator coil is re-energized, pulling the closest pole (positioned clockwise from the reference dot) to align with the red coil.

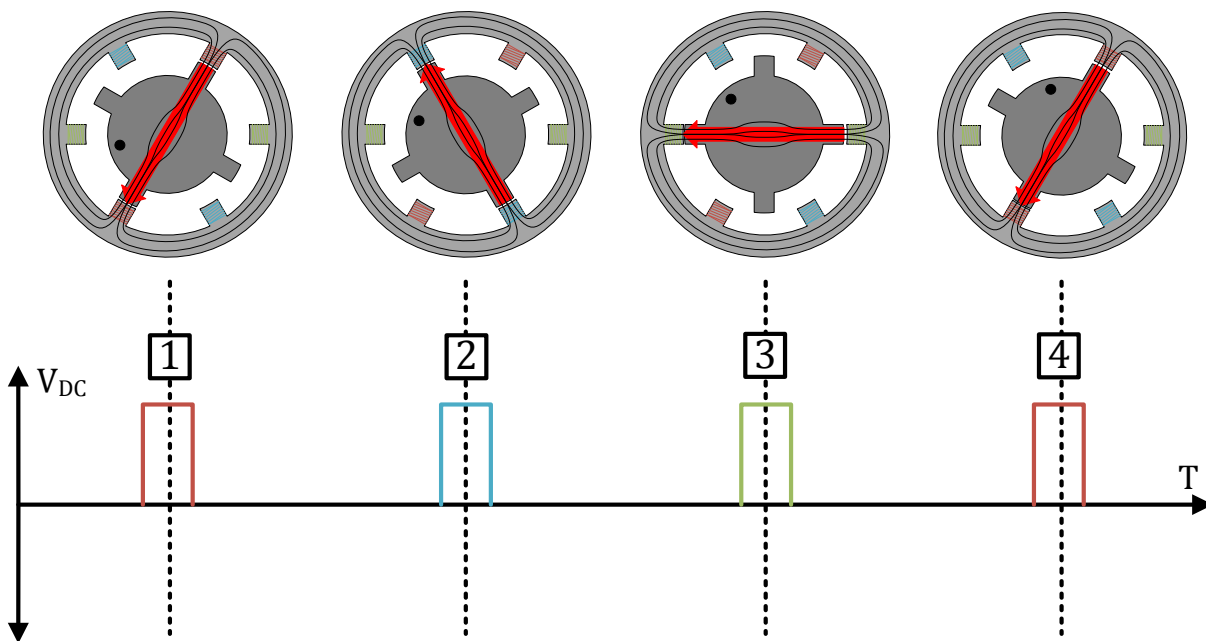


FIGURE 3: SIMPLE 6/4 SRM OPERATION DIAGRAM

The SRM's stator coil current typically flows in one direction, which can be counterintuitive when compared to an induction motor. Since magnetic reluctance will always pull the closest rotor pole, the movement is independent of the magnetic field orientation. Since the SRM uses a DC power supply, having the current flow in a single direction reduces the amount of circuitry needed to control the motor.

Unlike induction motors, SRMs are inherently variable-speed motors, since the stator coil current and switching frequency can be controlled separately. To control the motor over a range of speeds, the SRM drive must know the rotor orientation to properly time the stator coil commutation. Rotor orientation is typically measured using encoders or sensor-less methods developed by the manufacturer [9].

A new motor manufacturer claims to have developed a high rotor pole SRM, inverter, and patented control system that outperforms a National Electrical Manufacturers Association (NEMA) premium-rated motor at design and part loads. The increased number of rotor poles benefits motor performance by reducing torque ripple and generated acoustic noise [8].

Assessment Objectives

The objective of this project was to measure the performance of a nominal 3HP high rotor pole SRM with software-controlled inverter, and compare its performance to traditional induction motor technology. This emerging technology was compared to a nominal 3HP baseline induction motor with VFD in laboratory testing, and a nominal 3HP baseline single-speed induction motor in field testing.

For laboratory testing, motor performance was measured on a benchtop dynamometer and a laboratory RTU at a facility in Sunnyvale, California. The benchtop dynamometer testing measured performance at 49 different combinations of speed and torque. For laboratory RTU testing, the motors were installed on the RTU's indoor fan. Performance was measured at three different airflow resistances and seven different fan speeds.

For field testing, motor performance was monitored between November 1, 2017 and August 31, 2018, on a 10-ton RTU at a big box retail store in Corona, California. Testing was performed in three phases. The first phase tested the single-speed baseline motor. After baseline testing, the retrofit high rotor pole SRM was installed, and two additional tests were performed: 1) at a constant speed matching the baseline motor RPM; and 2) at a variable speed, to demonstrate further energy savings possible from implementing a variable-speed blower motor.

Finally, laboratory and field test results were used to calculate the average energy savings that could be achieved by installing the high rotor pole SRM in a 10-ton commercial RTU in SCE's service territory.

Technical Approach – Test Equipment

Baseline Equipment – Laboratory Testing

The standard nominal 3HP induction motor and VFD from a 10-ton commercial RTU (gas heat, refrigerant R-410A) with Multi-Stage Air Volume (MSAV) supply fan option was used as the baseline comparison for the high rotor pole SRM's motor performance. Table 1 provides the nameplate data for the baseline induction motor and VFD pair.

TABLE 1: NAMEPLATE DATA FOR LAB TEST BASELINE INDUCTION MOTOR AND VFD

Induction Motor	Value	VFD	Value
Horsepower	3	Horsepower	3
RPM	1725	Output Voltage	3-phase 480V
Frame	56-HZ	Output Type	3-phase Sine Wave
Power Factor	80%	Output Frequency	0.2-400HZ (PWM ¹)
NEMA Efficiency	84%	Power Factor	0.70
Enclosure	Open	Control	0-10V _{DC} Signal

¹Pulse width modulation

Baseline Equipment – Field Testing

Field testing was conducted on a 10-ton commercial RTU (gas heat, refrigerant R-22), which used a nominal 3HP three-phase constant-speed induction motor (Table 2).

TABLE 2: NAMEPLATE DATA FOR FIELD TEST BASELINE INDUCTION MOTOR

Induction Motor	Value
Horsepower	3
RPM	1725
Frame	56-HZ
Power Factor	72%-80% ¹
NEMA Efficiency	82%-88% ¹
Enclosure	Open

¹Exact number is proprietary

Emerging Technology Equipment – Laboratory and Field Testing

Emerging technology performance was characterized using a 3HP high rotor pole SRM and software-controlled inverter. Table 3 shows the nameplate data for the high rotor pole SRM and software-controlled motor and inverter.

TABLE 3: NAMEPLATE DATA FOR HIGH ROTOR POLE SRM

High Rotor Pole SRM	Value	Inverter	Value
Horsepower	3	Horsepower	3
RPM	1800	Output Voltage	680 V _{DC}
Frame	143T/145T ¹	Output Type	DC square wave
Power Factor	N/A ³	Output Frequency	100 – 300HZ ⁴
NEMA Efficiency	92%	Power Factor	65%
Enclosure	TEFC ²	Control	Digital

¹Motor was tested using the manufacturer's adapter to convert 143T/145T to 56HZ

²Totally Enclosed Fan Cooled (TEFC)

³SRMs use DC power and do not have a power factor

⁴For motor rotational speed range of 600 - 1800

Technical Approach – Laboratory Testing

Test Facility

The laboratory test facility was located in Sunnyvale, California. It consisted of a large, open shop space of approximately 40 feet wide by 50 feet long, with a 20-foot ceiling. It was oriented on a north-south axis (Figure 4). A 15-foot, uninsulated roll-up door (Figure 4, gray label) was centered on the south wall. A standard swing door (Figure 4, orange label) was adjacent to the roll-up door. A 10-ton commercial RTU, with MSAV supply fan option, was situated on a pair of two-foot-tall pallet shelves (Figure 4, green label) in the south-east corner. The shelves were arranged to ensure the supply and return openings were accessible. The RTU was connected to the manufacturer-specified three-phase power source via a wall connection.

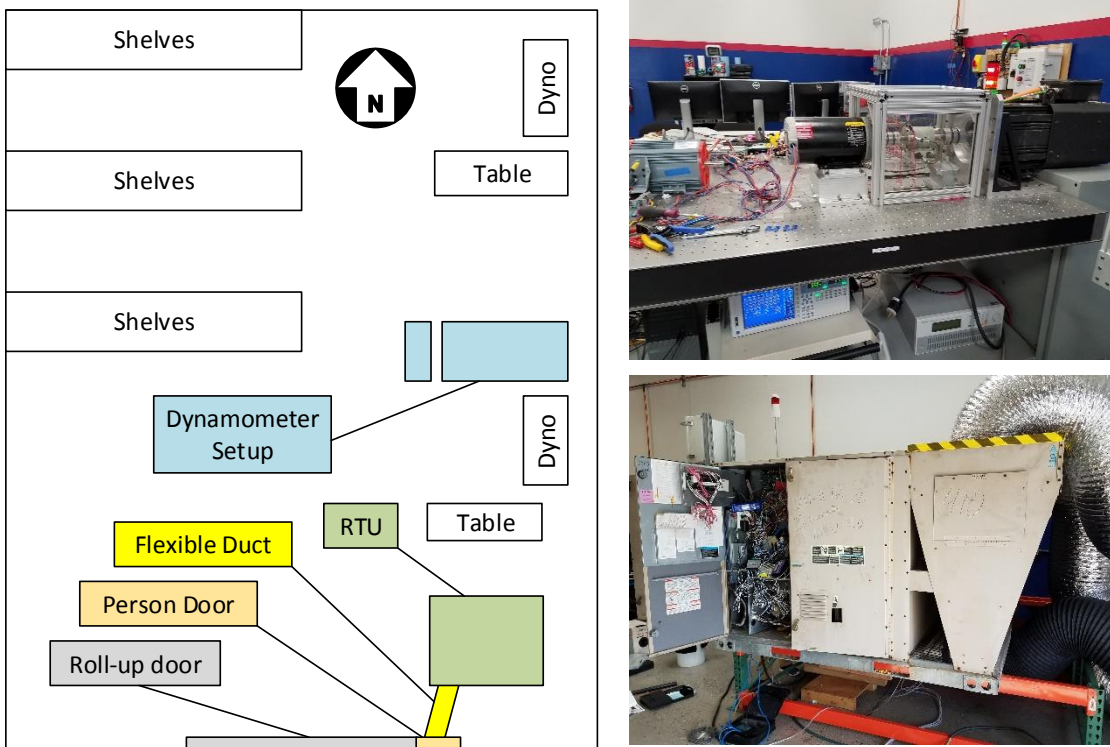


FIGURE 4: LAB FACILITY DIAGRAM (LEFT), DYNAMOMETER SETUP SOUTH FACE (TOP RIGHT), LAB RTU WEST FACE (LOWER RIGHT)

North of the RTU, several benchtop dynamometers were arranged as shown in Figure 4. The test dynamometer was aligned along the east-west axis, between the two other dynamometers (Figure 4, blue label).

Laboratory Benchtop Testing

Benchtop Dynamometer Overview

The benchtop dynamometer had the following components: combination torque meter and tachometer, power analyzer, load motor (13HP brushless AC servomotor), and custom control system (Figure 5). The test and load motors were both connected by the combination torque meter and tachometer.

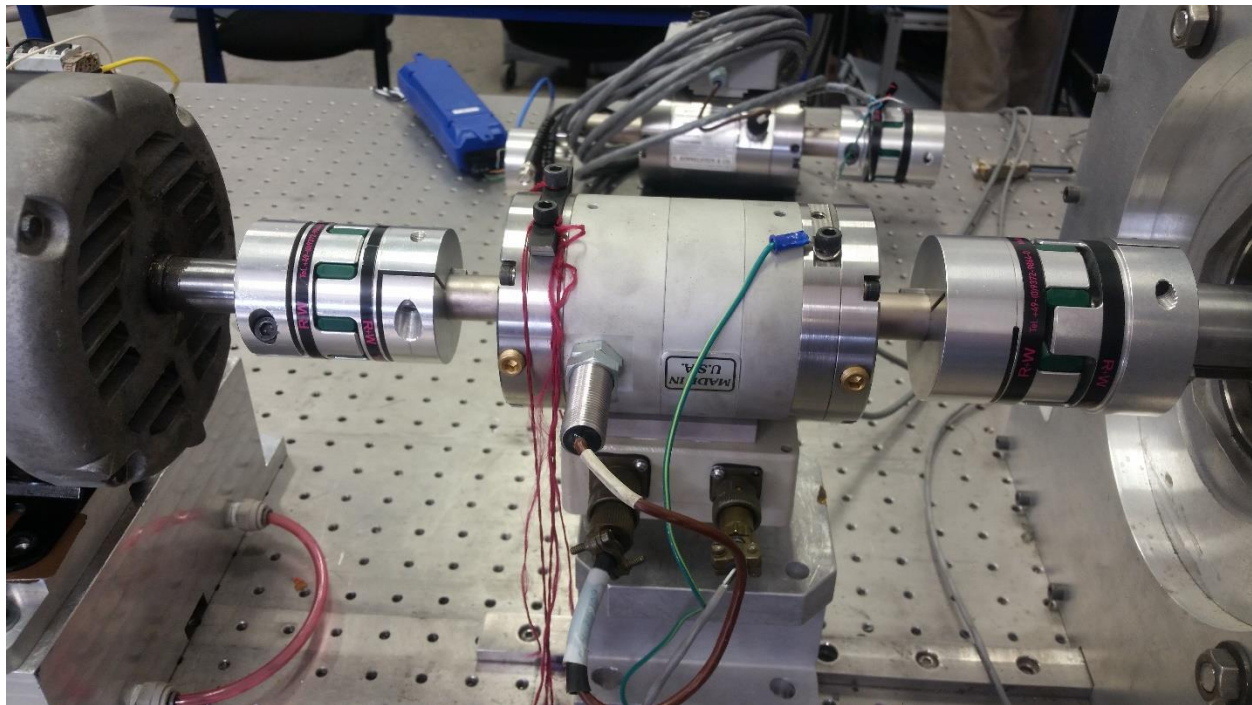


FIGURE 5: BASELINE MOTOR (LEFT) DYNAMOMETER SETUP

Benchtop Dynamometer Instrumentation

Table 4 describes the sensors used to monitor benchtop testing. All sensors were wired into the laboratory data acquisition, and were recorded at a frequency of 1HZ. The research team installed an additional three-phase power meter, to independently verify the system power measurement recorded by the laboratory data acquisition. Similar verification measurements were not possible for the torque and RPM readings, due to the dynamometer's construction.

TABLE 4: BENCHTOP MEASUREMENTS

Measurement Type	Manufacturer and Model #	Accuracy
System Power	Yokogawa WT1806-06-D-HE	$\pm(0.001\%$ reading $+0.005\%$ range)
Torque and Angular Speed (RPM)	S. Himmelstein MCRT 49702V(5-2)-C-F-Z (Signal read by Yokogawa)	$\pm(0.05\%$ reading $+0.05\%$ range)

Benchtop Dynamometer Test Procedures

Each motor's performance and drive was measured on the benchtop dynamometer over seven different load conditions at six different speeds, using the matrix shown in Table 5. Each test ran for about two minutes. The last minute of data for each test was used for the data analysis. The lowest operating speed was limited to 600 RPM by the default programming in the baseline VFD. To ensure the motors were warm, each ran for a minimum of 30 minutes prior to testing.

TABLE 5: BENCHTOP DYNAMOMETER TEST POINTS

		Speed						
		35%	42%	52%	62%	78%	100%	
LOAD	%	Nm	600 RPM	720 RPM	900 RPM	1075 RPM	1350 RPM	1725 RPM
	15	1.78	Test 01	Test 02	Test 03	Test 04	Test 05	Test 06
	25	2.95	Test 07	Test 08	Test 09	Test 10	Test 11	Test 12
	40	4.72	Test 13	Test 14	Test 15	Test 16	Test 17	Test 18
	50	5.91	Test 19	Test 20	Test 21	Test 22	Test 23	Test 24
	60	7.10	Test 25	Test 26	Test 27	Test 28	Test 29	Test 30
	75	8.86	Test 31	Test 32	Test 33	Test 34	Test 35	Test 36
	100	11.83	Test 37	Test 38	Test 39	Test 40	Test 41	Test 42

Laboratory RTU Testing

Laboratory RTU Overview

A 10-ton commercial RTU with an MSAV supply fan (gas heat, refrigerant R-410A) was used for laboratory testing (Figure 4, lower right). The research team used the test facility controls to mimic the thermostat control outputs. For all testing, the RTU was operated in fan-only mode, and an analog output signal was used to change the fan speed.

The research team built a supply plenum-duct apparatus to create three fixed-airflow resistance conditions and measure the airflow and static pressure during each test (Figure 6). A 20" x 20" x 28" plenum was built from 19/32" underlayment-grade plywood, and sealed with a combination of neoprene-EPDM-SBR foam, double-sided tape, and butyl mastic cord.

One 20" x 28" face of the plenum was left open and aligned with the 20" x 28" RTU supply air opening. Wooden pallets were placed under the plenum, to support and raise the plenum to the RTU's height. The plenum was attached to the RTU using 4" x 6" 28-gauge galvanized steel right-angle flashing. The flashing was secured to the wooden plenum with wood screws, and to the base of the RTU with sheet metal screws and a strip of neoprene-EPDM-SBR foam double-sided tape acting as a sealant.

One 20" x 20" side of the plenum had a 16" diameter hole where a quick-disconnect galvanized steel duct flange was attached using metal screws and a strip of neoprene-EPDM-SBR to seal the flange-plenum connection. A 20' section of 16" neoprene-coated polyester flexible duct, with 7" long 16" diameter duct extensions on either end, was connected to the plenum. The flexible duct was directed out of the warehouse through the pallet shelving under the RTU (Figure 6). The opening in the pallet shelving was slightly narrower than the duct itself, so the duct was slightly compressed between two of the metal supports (Figure 6). After exiting the pallet shelving, the duct made a $\sim 40^\circ$ turn out of the warehouse door to an outdoor parking lot, where it continued straight for the remainder of its length. The duct's final position was marked on the concrete, to ensure changes did not occur between tests.

Leaving the end of the duct open created the lowest external static pressure condition. The higher static pressure conditions were created by adding a custom orifice plate to the end of the duct, which increased the static pressure (Figure 7).

Holes were drilled in the duct portion of the flange and the duct extensions, to measure four-point space-average static pressure, temperature, RH, and standard volumetric flow rate of the air leaving the plenum (Figure 6 and Table 6).

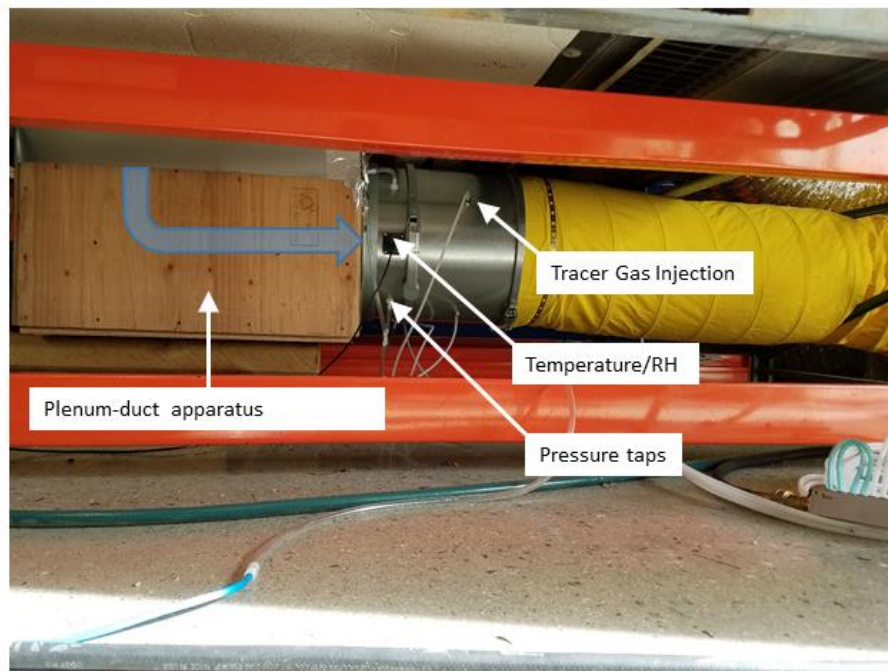


FIGURE 6: PLENUM-DUCT APPARATUS LAYOUT (WITH INSTRUMENTATION)

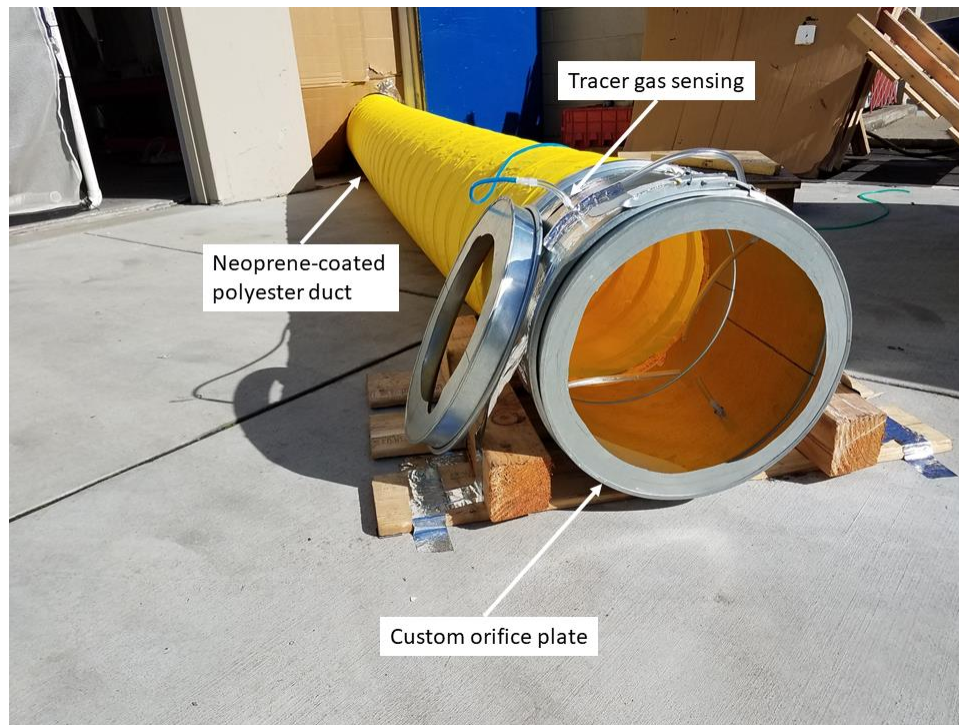


FIGURE 7: FLEXIBLE NEOPRENE-COATED POLYESTER DUCT LAYOUT (WITH INSTRUMENTATION)

Laboratory RTU Instrumentation

Table 6 describes the sensors used to measure the RTU's motor and drive performance.

TABLE 6: LABORATORY RTU TEST MEASUREMENTS

Symbol (Figure 8)	Measurement Type	Manufacturer and Model #	Accuracy
T/RH_{RA}	Return Air Temperature and RH	Vaisala HMP110	$\pm 0.1^{\circ}F$ $\pm 1.6\% RH$
T/RH_{SA}	Supply Air Temperature and RH	Vaisala HMP110	$\pm 0.1^{\circ}F$ $\pm 1.6\% RH$
ΔP_{FAN}	Air Differential Pressure across Fan (four pressure tap average)	TEC DG-1000	$\pm 0.8\%$ reading $\pm 0.05Pa$
ΔP_{ESP}	External Static Pressure (two pressure tap average)	TEC DG-1000	$\pm 0.8\%$ reading $\pm 0.05Pa$
-	Air Differential Pressure between the Laboratory and Outside	TEC DG-700	$\pm 1\%$ reading
Motor Speed	Angular Speed of the Motor Shaft	Nidec-Shimpo DT-2100	$\pm 0.006\%$ of reading
$POWER_{FAN}$	Electrical Power for VFD/Inverter and Motor	Dent PowerScout	1% of reading
$V_{AIRFLOW}$	CO ₂ Tracer Gas Airflow Measurement	WCEC	$\pm 2\%$ of reading

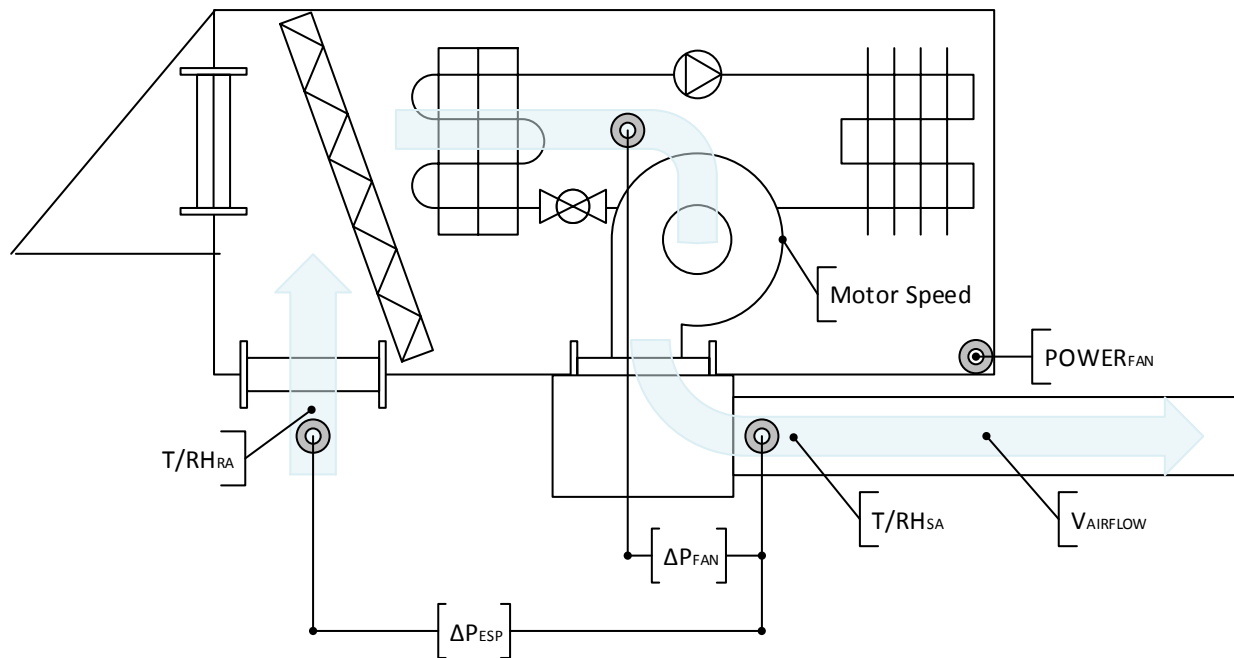


FIGURE 8: LABORATORY RTU INSTRUMENTATION LAYOUT SCHEMATIC

Air Temperature and Relative Humidity Measurements

Air temperature and RH were measured at the return air and supply air openings. These measurements were used in the air density calculations for measuring airflow through the RTU. The sensors were placed at the center of the return opening and the outlet of the plenum-duct cross-section.

Differential Pressure Measurements

Differential pressures were measured across the supply and return openings, from the interior laboratory space to the outdoor environment, and across the RTU's indoor fan.

Airflow Measurements

The RTU fan's airflow was measured with a tracer gas airflow measurement system, using carbon dioxide as the tracer. The gas was injected at the entrance of the neoprene-coated polyester flexible duct, and the resulting concentration change was measured between the return air opening and duct exit.

Motor Speed

The motor speed was measured with a handheld tachometer on a one-minute average. The tachometer was set up inside the fan cabinet. At the end of each several-minute-long steady-state test, the fan cabinet was opened, and the RPM average over the last minute was recorded.

Power Measurements

The electrical power each motor and drive system used was measured with a three-phase Root Mean Squared (RMS) power meter.

Data Acquisition System

Air temperature, RH, and power measurements were recorded with a dataTaker DT80 data logger. Airflow and pressure measurements were recorded using the sensor manufacturer's data logging programs on a laptop computer. The data logger and computer recorded data at a frequency of 1HZ. Motor speed measurements were recorded manually, at the end of each steady-state test. All data was combined into a single file, for post-processing and data analysis.

Laboratory RTU Test Procedures

Each motor was installed to drive the RTU's indoor fan through the existing belt configuration. Prior to testing, a belt tension measuring device, set to seven-pound-force, was used to ensure the fan drive belt was tensioned according to the manufacturer service manual (Figure 9) [10]. To warm up, each motor ran for a minimum of 30 minutes prior to testing.

Each motor was tested at the 21 test points defined in Table 7, which included three fixed-resistance conditions (0.4 inWC, 1.0 inWC, and 1.5 inWC) and seven different fan speeds. The three resistances were defined by the external static pressure (0.4 inWC, 1.0 inWC, and 1.5 inWC) when the baseline induction motor was running at 100% speed. At reduced speeds, the fixed-resistance condition (i.e., fixed duct system) resulted in a reduced external static pressure. Maximum airflow was determined by a one-time tracer gas airflow measurement taken while the baseline motor operated at 60HZ for each of the fixed-resistance conditions.

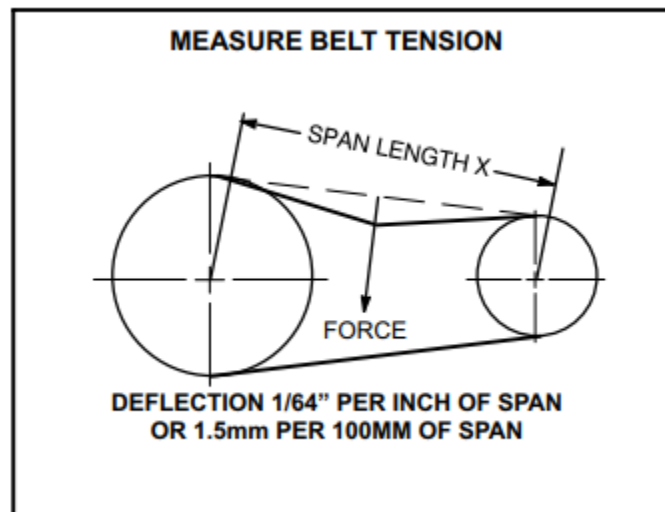


FIGURE 9: RTU MANUAL MEASURING BELT TENSION (IMAGE FROM [10])

TABLE 7: RTU TEST POINTS

		% of Maximum Airflow						
		100	90	80	70	60	50	40
Airflow Resistance	Low (0.4"WC @ 100% Airflow)	Test 01	Test 02	Test 03	Test 04	Test 05	Test 06	Test 07
	Med (1.0"WC @ 100% Airflow)	Test 08	Test 09	Test 10	Test 11	Test 12	Test 13	Test 14
	High (1.5"WC @ 100% Airflow)	Test 15	Test 16	Test 17	Test 18	Test 19	Test 20	Test 21

Equations and Error Analysis

The following section describes calculations for both the benchtop dynamometer testing and the laboratory RTU testing. For the benchtop dynamometer testing, the measured values of motor torque, speed, and electric power were used to calculate the motor/drive efficiency. For the laboratory RTU testing, the air temperature, RH, airflow, differential pressure, and electric power were used to calculate the combined fan/motor/drive efficiency and power intensity.

Benchtop Dynamometer Testing

For benchtop dynamometer testing, the motor output power was calculated using Equation 1.

EQUATION 1: MOTOR OUTPUT POWER

$$\text{Motor Output Power [W]} = \text{Motor Torque [N} \cdot \text{m]} * \text{Motor Speed [RPM]} * \frac{2\pi * 1 \text{ min}}{60 \text{ s}}$$

Where:

Motor Torque is the torque measured by the torque meter

Motor Speed is the speed measured by the tachometer

The motor efficiency was calculated using Equation 2.

EQUATION 2: MOTOR/DRIVE EFFICIENCY

$$\text{Motor|Drive Efficiency} = \frac{\text{Motor Output Power [W]}}{\text{System Input Power [W]}}$$

Where:

System Input Power is the electric power recorded by the power meter

Laboratory RTU Testing

For laboratory RTU testing, the airflow was calculated in real time using a high-accuracy, carbon dioxide (CO₂)-based, tracer gas airflow measurement system. The tests were conducted according to ASTM E2029, "Standard Test Method for Volumetric and Mass Flow Rate Measurement in a Duct Using Tracer Gas Dilution." This method mixed a measured mass flow rate of CO₂ into the supply air stream, and measured the corresponding rise in CO₂ downstream.

Those two values, along with background concentration of CO₂, were then used to calculate the volumetric airflow in standard units (Standard Cubic Feet per Minute [SCFM], Equation 3). The baseline CO₂ concentration, upstream of the injection point and the downstream CO₂ rise, was measured simultaneously.

EQUATION 3: TRACER GAS AIRFLOW MEASUREMENT CALCULATION

$$\dot{V}_{airflow} \left[\frac{std. ft^3}{min} \right] = \frac{\dot{V}_{CO_2} \left[\frac{std. ft^3}{min} \right]}{[CO_2]_{PPM, downstream} - [CO_2]_{PPM, baseline}}$$

Where:

$\dot{V}_{airflow}$ is the calculated volumetric airflow in SCFM

\dot{V}_{CO_2} is the measured volumetric flow rate of the carbon dioxide injected into the airstream

$[CO_2]_{PPM, downstream}$ is the measured carbon dioxide concentration in the air downstream of the injection point

$[CO_2]_{PPM, baseline}$ is the measured carbon dioxide concentration in the air upstream of the carbon dioxide injection

The result from Equation 3, along with the moist air density of the air measured during the test, was used to calculate the Actual Cubic Feet per Minute ([ACFM], Equation 4)

EQUATION 4: SCFM-TO-ACFM CONVERSION

$$ACFM \left[\frac{m^3}{min} \right] = \dot{V}_{airflow} \left[\frac{std. ft^3}{min} \right] * \frac{\rho_{standard} \left[\frac{lb_m}{std. ft^3} \right]}{\rho_{measured} \left[\frac{lb_m}{ft^3} \right]} * \frac{0.0283168 [m^3]}{1 [ft^3]}$$

Where:

$ACFM$ is actual airflow rate in cubic meters per minute

$\rho_{standard}$ is the moist air density of air at the standard conditions (14.696 psi, 70°F, 0% RH)

$\rho_{measured}$ is the moist air density of the air during the test, calculated using Equation 28 in ASHRAE Fundamentals 2005

Total pressure was calculated using static pressure measurements and the airflow rate measurements, and Equation 5.

EQUATION 5: TOTAL PRESSURE

$$\text{Total Pressure [Pa]} = \text{Static Pressure [Pa]} + \text{Dynamic Pressure [Pa]}$$

Where:

Static Pressure is the recorded measurement from the DG-1000, as shown in Figure 8 as ΔP_{FAN}

Dynamic Pressure is given by Equation 6

EQUATION 6: DYNAMIC PRESSURE

$$\text{Dynamic Pressure [Pa]} = \frac{1}{2} * \rho_{\text{measured}} \left[\frac{\text{kg}}{\text{m}^3} \right] * v^2 \left[\frac{\text{m}}{\text{s}} \right]$$

Where:

v is the velocity of the air at the point of the tracer gas injection given by Equation 7

EQUATION 7: AIRFLOW VELOCITY

$$v \left[\frac{\text{m}}{\text{s}} \right] = \frac{\text{ACFM} \left[\frac{\text{m}^3}{\text{min}} \right]}{\pi * r^2 [\text{m}]} * \frac{1 \text{ min}}{60 \text{ s}}$$

Where:

r is the radius of the duct at the point of the tracer gas injection (0.203 m)

Total pressure and airflow were used to calculate the resulting fan output power using Equation 8.

EQUATION 8: FAN OUTPUT POWER

$$\text{Fan Output Power [W]} = \text{Total Pressure [Pa]} * \text{ACFM} \left[\frac{\text{m}^3}{\text{min}} \right] * \frac{1 \text{ min}}{60 \text{ s}}$$

The combined fan/motor system efficiency was calculated using Equation 9.

EQUATION 9: FAN/MOTOR/DRIVE EFFICIENCY

$$\text{Fan|Motor|Drive Efficiency} = \frac{\text{Fan Output Power [W]}}{\text{System Input Power [W]}}$$

Finally, the power intensity of the fan and each motor/drive system was calculated using Equation 10.

EQUATION 10: FAN POWER INTENSITY

$$\text{Power Intensity} \left[\frac{\text{W}}{\text{ft}^3 / \text{min}} \right] = \frac{\text{System Input Power [W]}}{\text{ACFM} \left[\frac{\text{m}^3}{\text{min}} \right] * \frac{1 [\text{ft}^3]}{0.0283168 [\text{m}^3]}}$$

Measurement Uncertainty

The uncertainty of all calculations was computed with the sequential perturbation method. This is a numerical approach using a finite difference method to approximate derivatives to represent the sensitivity of the calculated value to the variables used in the calculation [11]. This method is well accepted, and is used when there is a complex partial differentiation method for the propagation of error, or there is a large number of variables.

The sequential perturbation process involves calculating a result (R_o) based on measured values. After R_o has been calculated, an independent variable within the R_o equation is perturbed by its respective uncertainty, and a new value (R_{i+}) is calculated. Next, the same independent variable within R_o is decreased by its respective uncertainty, and a new value (R_i) is calculated. The differences between R_{i+} and R_o , and R_i and R_o , are calculated, and the absolute values are averaged. The result is defined as δR_i . This process is repeated for every independent variable within R_o , and the final uncertainty is calculated as shown in Equation 11.

EQUATION 11: UNCERTAINTY USING SEQUENTIAL PERTURBATION

$$U_R = \pm \left[\sum_{i=1}^L (\delta R_i^2) \right]^{1/2}$$

Where:

δR_i is the calculated uncertainty for an independent variable

L is the total number of independent variables in a calculation

U_R is the total calculated uncertainty

Results – Laboratory Testing

Benchtop Dynamometer Testing

The results for system efficiency, torque versus power, and power factor illustrate that the high rotor pole SRM with software-controlled inverter had improved performance over all the test points when compared to the baseline induction motor and VFD. Figure 10, Figure 11, and Figure 12 illustrate the trends for each of the three metrics along with a best-fit line. Each figure has six subplots, one for each six RPM test conditions. For all the figures and plots, torque increases with power from left to right. Table 8 through Table 13 provides a summary of each point in the figures.

Motor/Drive Efficiency

The dynamometer test result show the high rotor pole SRM system had a higher motor/drive efficiency over all the test points compared to the baseline system (Figure 10). Both systems demonstrated a trend of increasing efficiency as the power input increased. The motor/drive efficiency of the high rotor pole SRM was between 73%-91%, while the baseline system ranged from 46%-81% (Table 8 and Table 9).

Overall, the high rotor pole SRM efficiency was between 10% and 57% higher than the baseline. The greatest efficiency increase was seen at 600 RPM and 1.75 Nm, and the least at 1,725 RPM and 11.8 Nm, which corresponds to the test points with the smallest and largest loads, respectively.

Torque versus Power

Figure 11 illustrates the relationship between torque and power for the high rotor pole SRM and baseline systems, at each RPM test condition. As expected, both motors consumed more power as RPM and torque increased.

The most significant improvement was observed at the 600 RPM and 1.75 Nm test point, where the baseline system used 235 watts compared to the high rotor pole SRM system's 150 watts – a 36.2% reduction in power to generate the same motor output. The smallest improvement was observed at the 1,725 RPM and 11.8 Nm test point, where the baseline system used 2,614 Watts and the high rotor pole SRM system used 2,374 Watts, a 9.2% reduction in power to achieve the same motor output.

Power Factor

Both the baseline and high rotor pole SRM systems had power factors that trended upward as the power draw increased. Over all of the test points, the power factors for the baseline and high rotor pole SRM were in the range of 0.46 – 0.68 and 0.42 – 0.67, respectively (Table 12 and Table 13). The baseline had a power factor that was higher than the high rotor pole SRM in 32/42 tests, equal to the high rotor pole SRM for 9/42 tests, and less than the high rotor pole SRM in only 1/42 tests.

The biggest difference in power factor was measured (9.5%) at the 600 RPM and 1.75 Nm test point. The high rotor pole SRM system had a greater power factor only at the 720 RPM and 2.95 Nm test point.

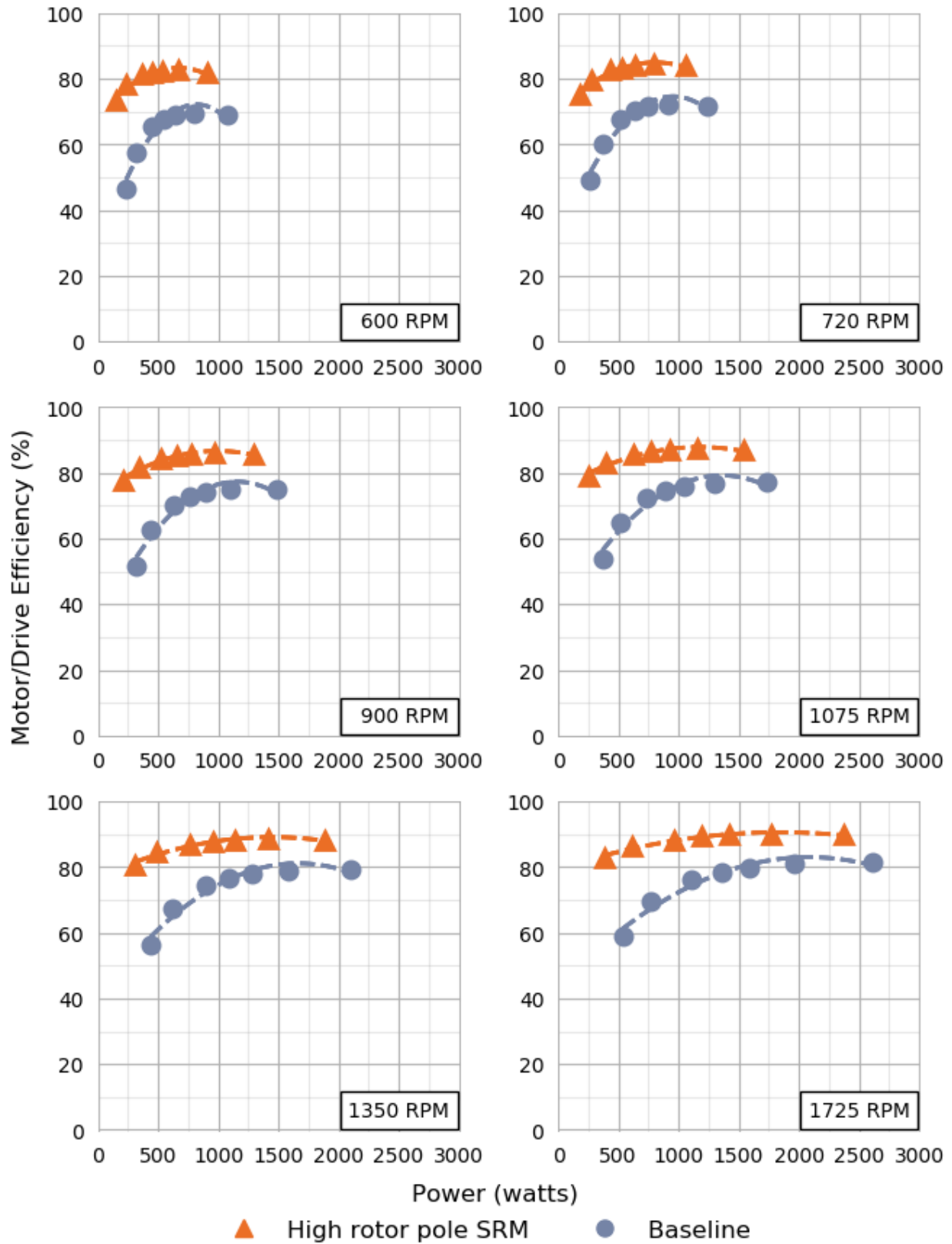


FIGURE 10: POWER VS. MOTOR/DRIVE EFFICIENCY FOR BENCHTOP DYNAMOMETER TEST WITH 2ND-ORDER POLYNOMIAL FIT

TABLE 8: BASELINE SYSTEM MOTOR/DRIVE EFFICIENCY SUMMARY TABLE (EFFICIENCY AT EACH CONDITION)

		Torque (Nm)						
		1.75	2.95	4.72	5.91	7.08	8.86	11.8
Motor Speed	600 RPM	46%	58%	65%	68%	69%	70%	69%
	720 RPM	49%	60%	68%	70%	71%	72%	72%
	900 RPM	52%	63%	70%	73%	74%	75%	75%
	1,075 RPM	54%	65%	72%	75%	76%	77%	77%
	1,350 RPM	59%	67%	74%	77%	78%	79%	79%
	1,725 RPM	59%	70%	76%	79%	80%	81%	81%

TABLE 9: HIGH ROTOR POLE SRM SYSTEM MOTOR/DRIVE EFFICIENCY SUMMARY TABLE (EFFICIENCY AT EACH CONDITION)

		Torque (Nm)						
		1.75	2.95	4.72	5.91	7.08	8.86	11.8
Motor Speed	600 RPM	73%	78%	81%	82%	82%	83%	82%
	720 RPM	75%	80%	83%	83%	84%	84%	84%
	900 RPM	78%	82%	84%	85%	86%	86%	86%
	1,075 RPM	79%	83%	85%	87%	87%	87%	87%
	1,350 RPM	81%	85%	87%	88%	88%	89%	88%
	1,725 RPM	83%	86%	88%	89%	90%	90%	90%

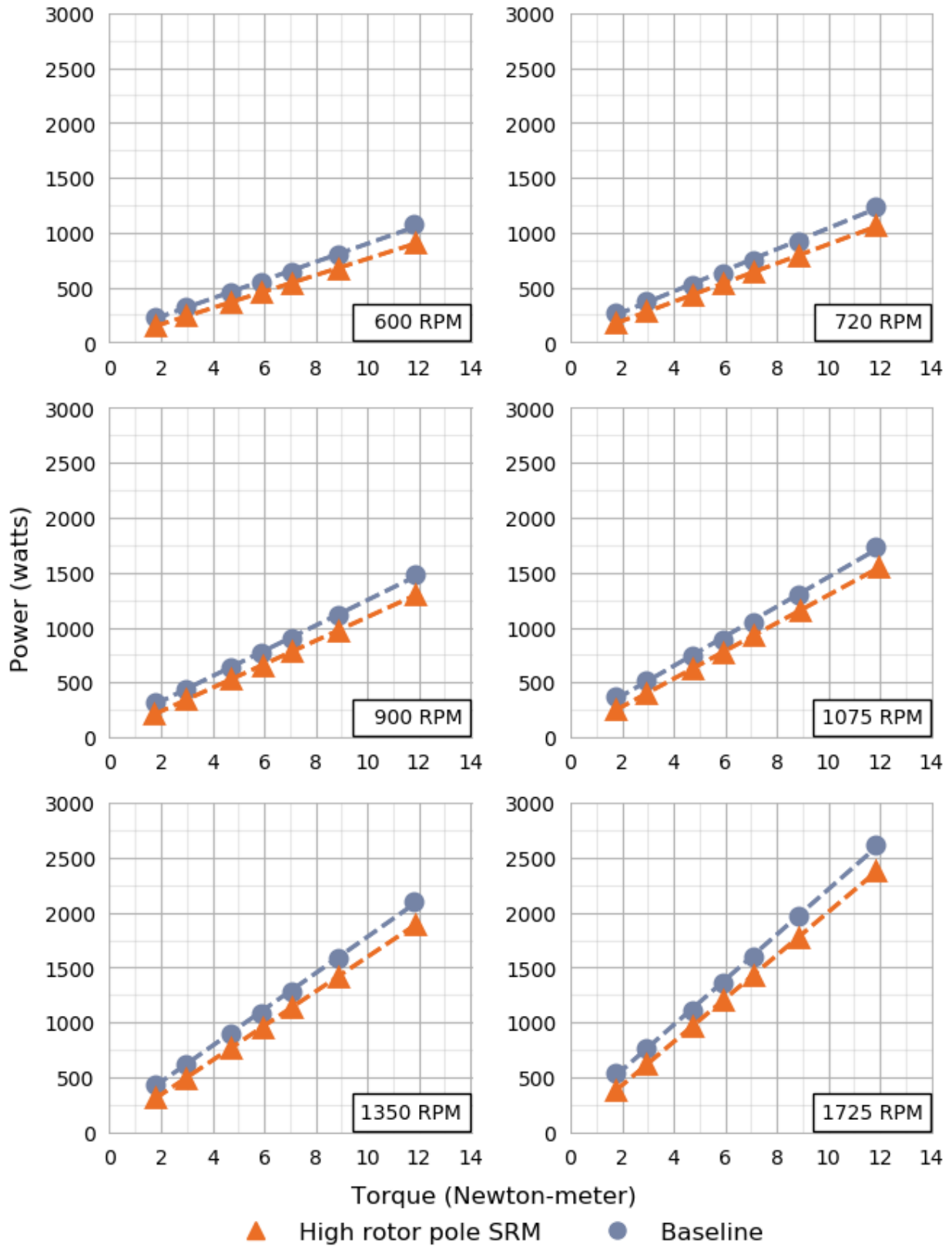


FIGURE 11: TORQUE VS. POWER FOR BENCHTOP DYNAMOMETER TEST WITH LINEAR FIT

TABLE 10: BASELINE SYSTEM MOTOR/DRIVE POWER SUMMARY TABLE (WATTS AT EACH CONDITION)

		Torque (Nm)						
		1.75	2.95	4.72	5.91	7.08	8.86	11.8
Motor Speed	600 RPM	235	320	452	545	641	796	1073
	720 RPM	269	370	522	633	745	920	1240
	900 RPM	320	442	630	762	899	1108	1484
	1,075 RPM	368	513	737	893	1050	1297	1729
	1,350 RPM	440	620	896	1088	1283	1582	2101
	1,725 RPM	537	766	1113	1357	1595	1967	2614

TABLE 11: HIGH ROTOR POLE SRM SYSTEM MOTOR/DRIVE POWER SUMMARY TABLE (WATTS AT EACH CONDITION)

		Torque (Nm)						
		1.75	2.95	4.72	5.91	7.08	8.86	11.8
Motor Speed	600 RPM	150	238	367	453	539	673	904
	720 RPM	176	280	434	534	636	789	1059
	900 RPM	212	340	528	654	778	969	1297
	1,075 RPM	251	402	656	773	922	1152	1546
	1,350 RPM	308	491	769	954	1135	1416	1890
	1,725 RPM	383	617	965	1195	1425	1776	2374

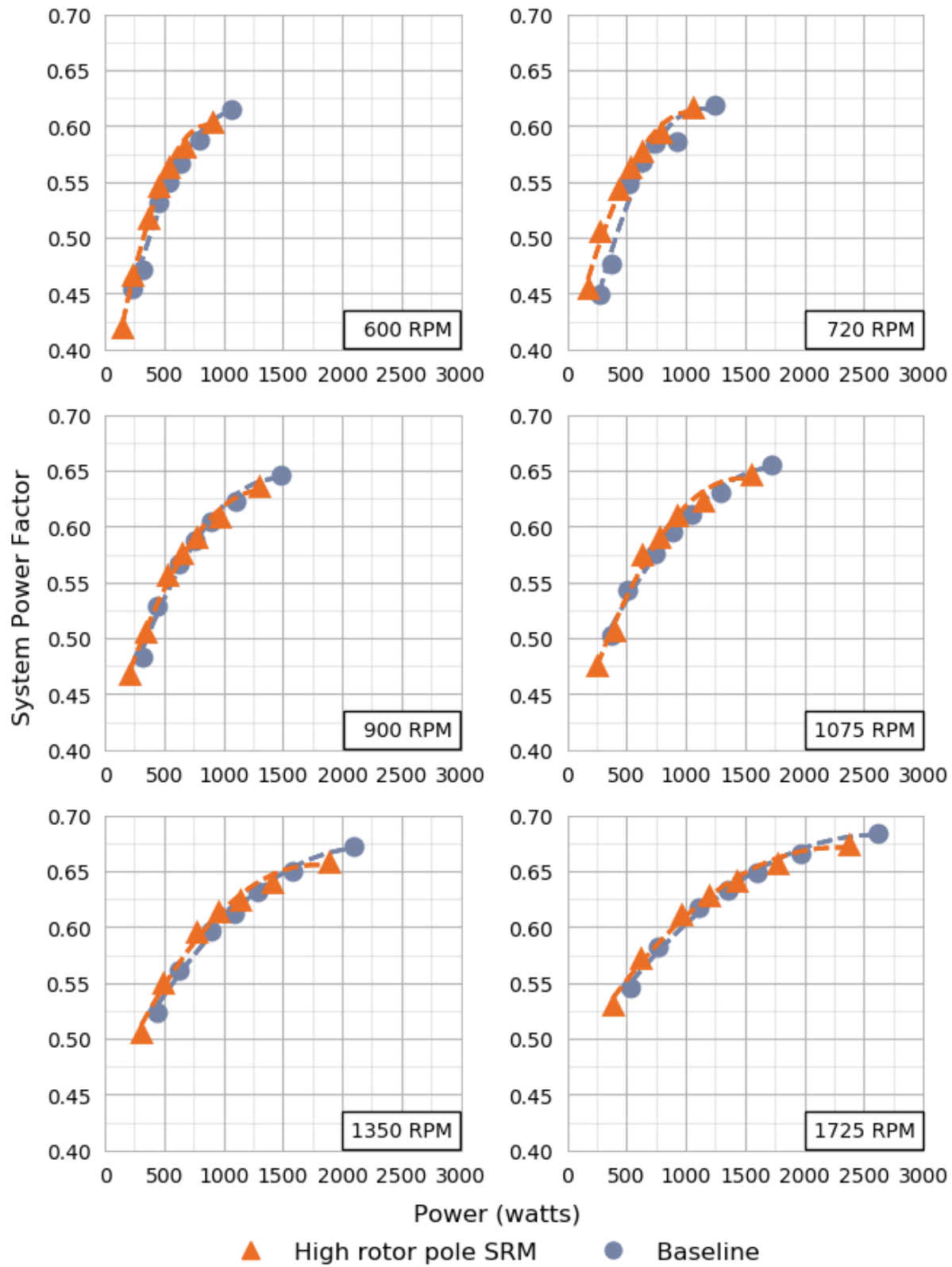


FIGURE 12: POWER VS. MOTOR/DRIVE POWER FACTOR FOR DYNAMOMETER TESTING WITH 2ND-ORDER POLYNOMIAL FIT

TABLE 12: BASELINE SYSTEM MOTOR/DRIVE POWER FACTOR SUMMARY TABLE (POWER FACTOR AT EACH CONDITION)

		Torque (Nm)						
		1.75	2.95	4.72	5.91	7.08	8.86	11.8
Motor Speed	600 RPM	0.46	0.47	0.53	0.55	0.57	0.59	0.61
	720 RPM	0.45	0.48	0.55	0.57	0.59	0.59	0.62
	900 RPM	0.48	0.53	0.57	0.59	0.60	0.62	0.65
	1,075 RPM	0.50	0.54	0.58	0.60	0.61	0.63	0.66
	1,350 RPM	0.52	0.56	0.60	0.61	0.63	0.65	0.67
	1,725 RPM	0.55	0.58	0.62	0.63	0.65	0.67	0.68

TABLE 13: HIGH ROTOR POLE SRM SYSTEM MOTOR/DRIVE POWER FACTOR SUMMARY TABLE (POWER FACTOR AT EACH CONDITION)

		TORQUE (NM)						
		1.75	2.95	4.72	5.91	7.08	8.86	11.8
Motor Speed	600 RPM	0.42	0.47	0.52	0.55	0.56	0.58	0.60
	720 RPM	0.45	0.50	0.54	0.56	0.58	0.59	0.62
	900 RPM	0.47	0.51	0.56	0.58	0.59	0.61	0.64
	1,075 RPM	0.48	0.51	0.57	0.59	0.61	0.62	0.65
	1,350 RPM	0.51	0.55	0.60	0.61	0.62	0.64	0.66
	1,725 RPM	0.53	0.57	0.61	0.63	0.64	0.66	0.67

Combined Fan/Motor/Drive Efficiency

RTU lab test results demonstrate an opportunity for the high rotor pole SRM system to save energy when compared to the baseline system. As expected, both motors operated with a higher fan/motor/drive efficiency as the airflow rate and airflow resistance increased (Figure 13, Table 14, and Table 15). Additionally, the high rotor pole SRM had a higher fan/motor/drive efficiency across all static pressures and airflow rates.

Average efficiency increases were 26%, 23%, and 28% for the low, medium, and high-airflow resistance tests. The greatest improvement (+57%) was measured at the lowest airflow rate of the high-airflow resistance tests. The smallest efficiency gain was measured at the 90% airflow condition of the medium-airflow resistance test (+8%).

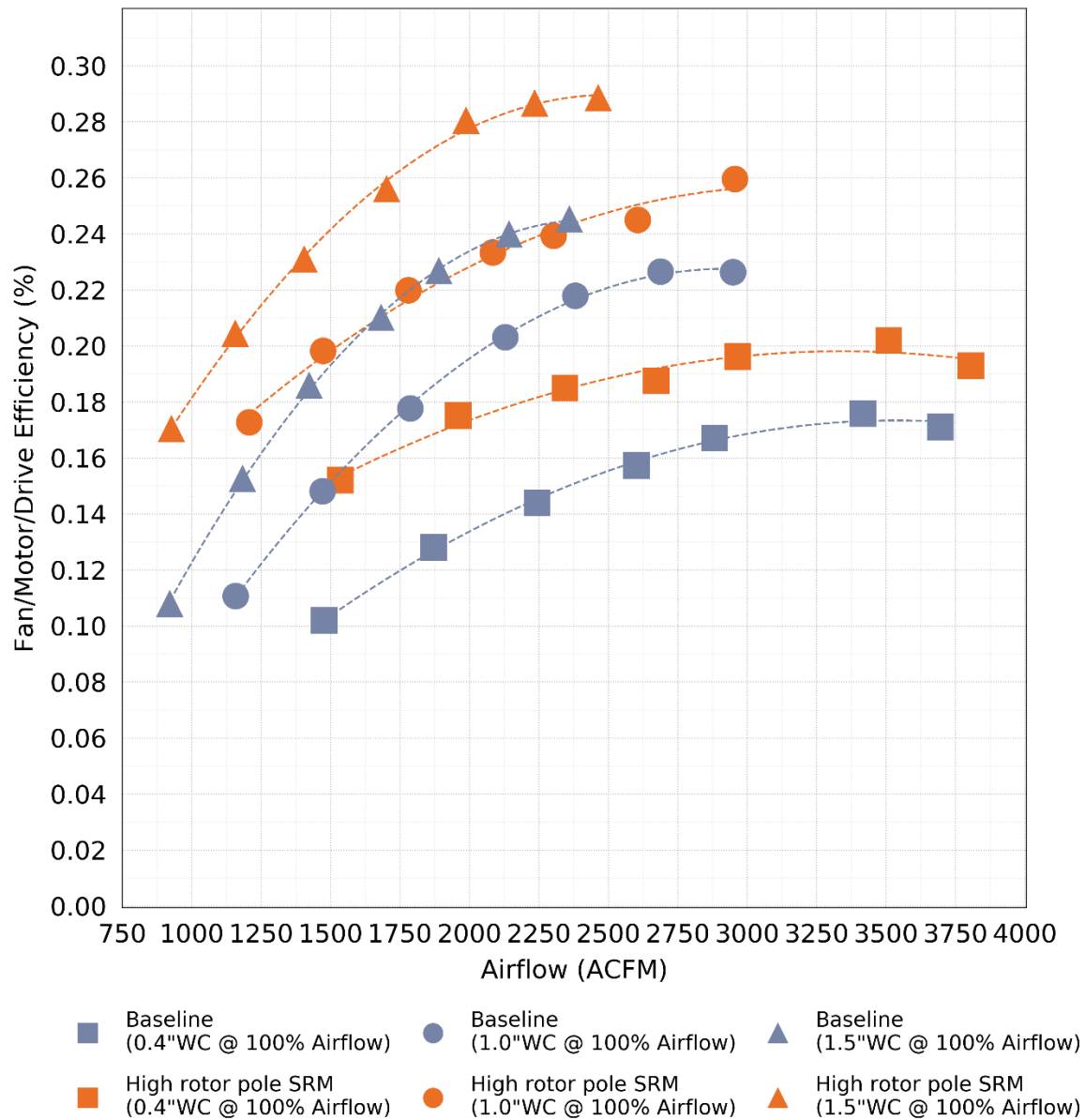


FIGURE 13: AIRFLOW VS. FAN/MOTOR/DRIVE EFFICIENCY FOR LAB RTU TEST

TABLE 14: BASELINE SYSTEM FAN/MOTOR/DRIVE EFFICIENCY SUMMARY TABLE (EFFICIENCY AT EACH CONDITION)

		% of Maximum Airflow						
		100	90	80	70	60	50	40
Airflow Resistance	Low (0.4"WC @ 100% Airflow)	17.1%	17.6%	16.7%	15.7%	14.4%	12.8%	10.2%
	Medium (1.0"WC @ 100% Airflow)	22.6%	22.7%	21.8%	20.3%	17.8%	14.8%	11.1%
	High (1.5"WC @ 100% Airflow)	24.5%	24.0%	22.7%	21.0%	18.6%	15.3%	10.8%

TABLE 15: HIGH ROTOR POLE SRM SYSTEM FAN/MOTOR/DRIVE EFFICIENCY SUMMARY TABLE (EFFICIENCY AT EACH CONDITION)

		% of Maximum Airflow						
		100	90	80	70	60	50	40
Airflow Resistance	Low (0.4"WC @ 100% Airflow)	19.3%	20.2%	19.6%	18.8%	18.5%	17.5%	15.2%
	Medium (1.0"WC @ 100% Airflow)	26.0%	24.5%	23.9%	23.3%	22.2%	19.8%	17.3%
	High (1.5"WC @ 100% Airflow)	28.8%	28.7%	28%	25.6%	23.1%	20.4%	17.0%

Fan Power Intensity

Fan power intensity describes the amount of power (in watts) consumed per volume of air moved (in ACFM). A lower value indicates the fan system is operating more efficiently, because it is using less power to move air.

For both motors, fan power intensity increased as airflow and airflow resistance increased (Figure 14, Table 16, and Table 17). This result was expected, because the power needed to drive the fan was proportional to the cubic of the air velocity, and the duct size was constant for all tests. In the low, medium, and high-airflow resistance tests, the high rotor pole SRM lowered the power intensity by 16.9%, 17.5%, and 21.3% respectively. The biggest reduction in fan power intensity was 36.1%, measured at the 100% flow point of the high-airflow resistance test. The smallest reduction was 9%, measured at the 90% flow point of the medium-airflow resistance test.

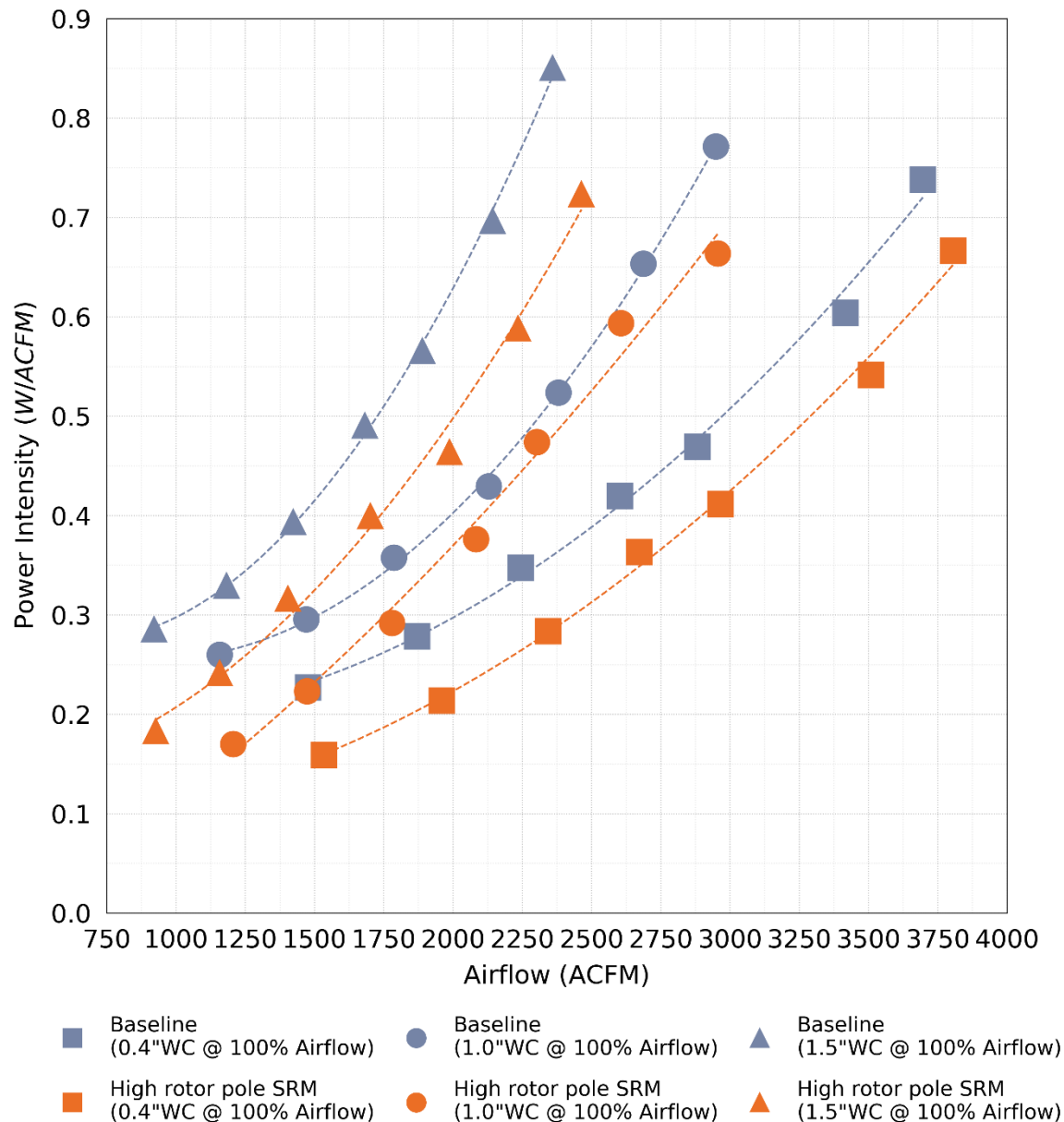


FIGURE 14: AIRFLOW VS. POWER INTENSITY FOR LABORATORY RTU TESTING

TABLE 16: BASELINE SYSTEM POWER INTENSITY SUMMARY TABLE

		% of Maximum Airflow						
		100	90	80	70	60	50	40
Airflow Resistance	Low (0.4"WC @ 100% Airflow)	0.738	0.603	0.469	0.421	0.348	0.278	0.230
	Medium (1.0"WC @ 100% Airflow)	0.773	0.654	0.524	0.430	0.357	0.295	0.261
	High (1.5"WC @ 100% Airflow)	0.848	0.697	0.566	0.490	0.394	0.329	0.286

TABLE 17: HIGH ROTOR POLE SRM SYSTEM POWER INTENSITY SUMMARY TABLE

		% of Maximum Airflow						
		100	90	80	70	60	50	40
Airflow Resistance	Low (0.4"WC @ 100% Airflow)	0.666	0.542	0.411	0.363	0.284	0.213	0.160
	Medium (1.0"WC @ 100% Airflow)	0.665	0.595	0.474	0.376	0.292	0.223	0.170
	High (1.5"WC @ 100% Airflow)	0.722	0.587	0.464	0.400	0.316	0.242	0.183

Uncertainty

The uncertainty for torque, speed, motor/drive efficiency, airflow, power, fan output, and fan/motor/drive efficiency was calculated for typical values, and is listed in Table 18. The uncertainty of the calculated metrics did not impact the laboratory testing results.

TABLE 18: UNCERTAINTIES FOR TYPICAL VALUES

Metric	Typical Value	Uncertainty
Torque (Nm)	1.013	±0.0367
Speed (RPM)	723	±12.03
Motor/Drive Efficiency (%)	67.9	±3.69
Airflow (ACFM)	3700	±81.4
Power (kW)	2.73	±0.027
Fan Output Power (W)	349	±14.4
Motor/Drive/Fan Efficiency (%)	0.128	±0.0054

Power Intensity (W/ACFM)	0.73	±0.017
--------------------------	------	--------

Summary – Laboratory Testing

Benchtop dynamometer and laboratory RTU test results show the high rotor pole SRM with software-controlled inverter is a promising option for reducing fan power in commercial RTUs, when compared to an equivalent-sized induction motor.

In dynamometer testing, the high rotor pole SRM used 9.2% to 36.2% less power than the induction motor and VFD system to generate the same torque. Additionally, the difference in the power factor between the two systems was no more than 10% for all test points, so the high rotor pole SRM was not expected to affect overall system electrical performance.

In laboratory testing, the high rotor pole SRM reduced fan power intensity when retrofitted to the existing belt and fan configuration. On average, the high rotor pole SRM reduced fan power intensity by 16.9%, 17.5%, and 21.3% for low, medium, and high-airflow resistance conditions.

Technical Approach – Field Testing

Site and Unit Selection

A big box retail store in Corona, California was selected for field testing the high rotor pole SRM, because the research team had already installed instrumentation on a suitable RTU that was previously used for another emerging technology project. The store was cooled by several packaged RTUs with a nominal tonnage of 3-20, for a total of 262 tons of cooling. The selected field test RTU is highlighted in Figure 15.

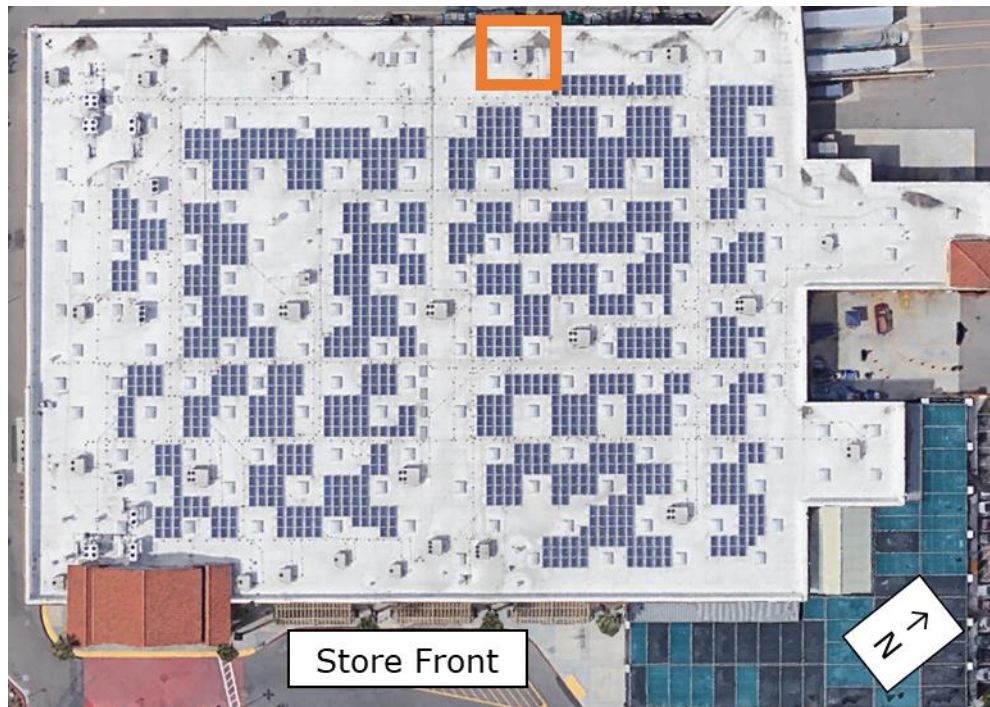


FIGURE 15: BIRD'S EYE VIEW OF FIELD TEST SITE (ORANGE SQUARE SHOWS RTU 24 LOCATION)

Field Testing Overview

Field testing occurred in three phases. This allowed the research team to measure energy savings resulting from the high rotor pole SRM's improved efficiency, plus the additional energy savings that could be achieved by using variable-speed controls.

In Phase I, baseline testing was performed with the original 3HP single-speed induction motor, which operated at 1,725 RPM regardless of RTU mode. At this motor speed, the fan operated at 715 RPM. Next, the emerging technology 3HP high rotor pole SRM was installed, together with its software-controlled inverter. In Phase II, the motor was programmed to run the indoor fan at the same fixed speed as the baseline. In Phase III, the high rotor pole SRM was operated at variable speeds, based on manufacturer recommendations for RTU operating mode (Table 19). Chronologically, Phase III was tested before Phase II; however, the test order was not expected to impact results.

TABLE 19: FIELD TEST PHASES

	Phase I	Phase II	Phase III
Motor	Baseline 3HP induction motor – fixed speed	Retrofit 3HP high rotor pole SRM – fixed speed	Retrofit 3HP high rotor pole SRM – variable speed controls
Testing Period	11/01/2017 – 02/04/2018	03/23/2018 – 08/31/180	2/07/2018 – 03/22/2018
Air Circulation Motor Speed (RPM)	1725	1725	690
Air Circulation Fan Speed (RPM)	715	715	283
Cool 1 Motor Speed (RPM)	1725	1725	1294
Cool 1 Fan Speed (RPM)	715	715	531
Cool 2 Motor Speed (RPM)	1725	1725	1725
Cool 2 Fan Speed (RPM)	715	715	715

Instrumentation

Table 20 and Figure 16 describe the sensors used to monitor each motor’s performance, as well as a general outline of where the sensors were installed. All sensors were wired directly to a dataTaker 85M data acquisition system. The data was sampled at one-minute intervals, and daily data files were transferred to a remote FTP server each night, for the duration of the monitoring period.

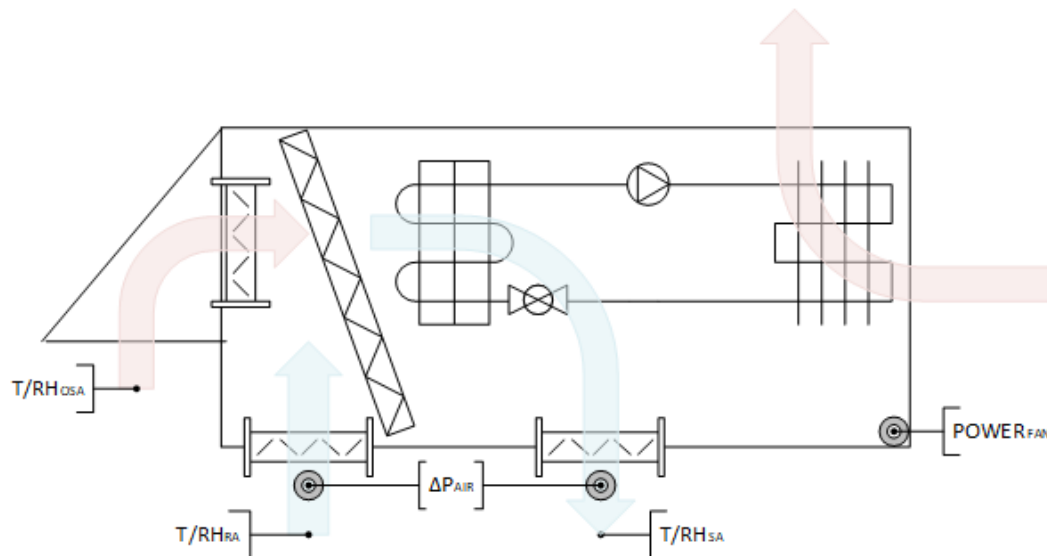


FIGURE 16: FIELD TEST INSTRUMENTATION SCHEMATIC

TABLE 20: FIELD TEST MEASUREMENTS

Symbol (Figure 16)	Measurement Type	Manufacturer and Model #	Accuracy	Signal Type
T _{OSA}	Outside Air Temperature	Vaisala HMP110	±0.1°F	Analog
RH _{OSA}	Outside Air RH	Vaisala HMP110	±1.6%	Analog
T _{SA}	Supply Air Temperature	Vaisala HMP110	±0.1°F	Analog
RH _{SA}	Supply Air RH	Vaisala HMP110	±1.6%	Analog
T _{RA}	Return Air/Indoor Temperature	Vaisala HMP110	±0.1°F	Analog
RH _{RA}	Return Air/Indoor RH	Vaisala HMP110	±1.6%	Analog
ΔP _{AIR}	Supply Air Differential Pressure (Mapped to Airflow)	Dwyer	± 0.0025 "WC	Analog
Power _{FAN}	Fan Power	Dent PowerScout	1% of reading	RS-485

Air Temperature and Relative Humidity Measurements

Air temperature and RH was measured using a single temperature and an RH sensor placed in the desired airstream. Each sensor was placed near the center of the airstream, to minimize any wall effects from the ducting.

One-Time Tracer Gas Airflow Map Measurement

The field test unit's airflow was mapped to the differential pressure measurement during a one-time field evaluation using a high-accuracy, carbon dioxide (CO₂)-based, tracer gas airflow measurement system. The tests were conducted according to ASTM E2029 "Standard Test Method for Volumetric and Mass Flow Rate Measurement in a Duct Using Tracer Gas Dilution" [12]. This method mixes a measured mass flow rate of CO₂ into the supply air stream, and measures the corresponding rise in CO₂ concentration downstream. Those two values, along with the background CO₂ concentration, are then used to calculate the duct's volumetric airflow in standard units (SCFM, Equation 3).

Since the baseline induction motor operated at a fixed speed, the research team generated a system fan curve by removing the filters (or blocking parts of the filters with cardboard) to simulate five different airflow resistance points. The resistance points corresponded to taking airflow measurements without filters, with filters, blocking 25% of the filter area, blocking 50% of the filter area, and blocking 80% of the filter area. After the high rotor pole SRM was installed, the research team used the motor's control system to operate the fan at different speeds.

Differential Pressure Measurement

Differential pressure was measured between the supply and return ducts. The measurement included the pressure drop across the air filters and evaporator coil.

Power Measurement

RTU electrical power was measured using a three-phase RMS power meter installed on the indoor fan motor's power supply. The power meter measured true power, reactive power, apparent power, power factor, voltage, and current for all three power phases.

Data Acquisition System

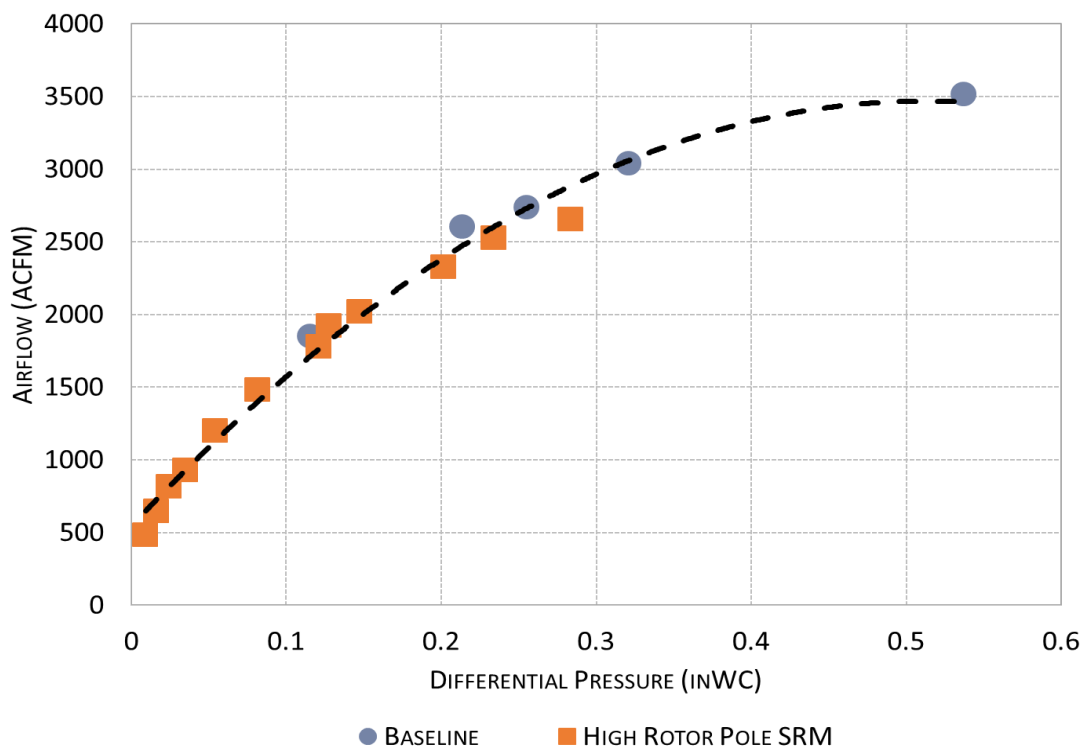
Air temperature, RH, differential pressure, and power measurements were recorded with a dataTaker DT85M data logger, which recorded data at a frequency of one sample per minute.

Equations and Error Analysis

In field testing, the airflow (measured in SCFM and ACFM) was calculated using the same methods as in laboratory testing, as described by Equation 3 and Equation 4.

The airflow in ACFM (measured only during the test setup) was correlated to external static pressure (measured continuously) using the best quadratic fit (Figure 17). Equation 12 describes the best fit result of the airflow map, and was used to estimate minute-by-minute airflow during the field test. As expected, the motor change did not affect the relationship between differential pressure and airflow.

FIGURE 17: RESULTS OF ONE-TIME TRACER GAS AIRFLOW MAP TO DIFFERENTIAL PRESSURE BETWEEN SUPPLY AND RETURN DUCTS



EQUATION 12: FIELD TEST AIRFLOW MAP

$$ACFM \left[\frac{ft^3}{min} \right] = x_0 * ESP^2 [inWC] + x_1 * ESP [in WC] + x_2$$

$$x_0 = -11142.67154887150000$$

$$x_1 = 11417.52263931930000$$

$$x_2 = 543.43934443448800$$

Where:

ESP is the measured external static pressure, as shown in Figure 16 as ΔP_{AIR}

Finally, fan and motor power intensity was calculated using the same methods as in laboratory testing (Equation 10).

Measurement Uncertainty

The uncertainty of all calculations was computed using the sequential perturbation method, as described under Measurement Uncertainty in the Technical Approach – Laboratory Testing section of this document.

Results – Field Testing

Airflow

Loading air filters over time severely impacted the system’s airflow. It increased airflow resistance and decreased overall airflow. The airflow range for each field test phase is shown in Table 21 and the hourly average for the entire study is shown in Figure 18. The filter loading in June-July of 2018 was impacted by poor air quality from wildfires in the local area. Additionally, as the airflow dropped, the amount of condensate on the evaporator coil increased, further raising the airflow resistance.

Data from between June 1, 2018 and July 16, 2018 was excluded from the final analysis, because significant airflow and power reductions skewed the high rotor pole SRM results to be abnormally low.

TABLE 21: AIRFLOW RANGE OBSERVED DURING VARIOUS TEST PHASES

	Phase I	Phase II	Phase III
Motor	Baseline 3HP induction motor – fixed speed	Retrofit 3HP high rotor pole SRM – fixed speed	Retrofit 3HP high rotor pole SRM – variable speed controls
Testing Period	11/01/2017 – 02/04/2018	03/23/2018 – 08/31/180	2/07/2018 – 03/22/2018
Airflow Range (ACFM)	1752 - 3467	1319 - 3468	837 - 3387
Hourly Average Airflow Range (ACFM)	2520 – 3446	2467 – 3353	899 – 3227

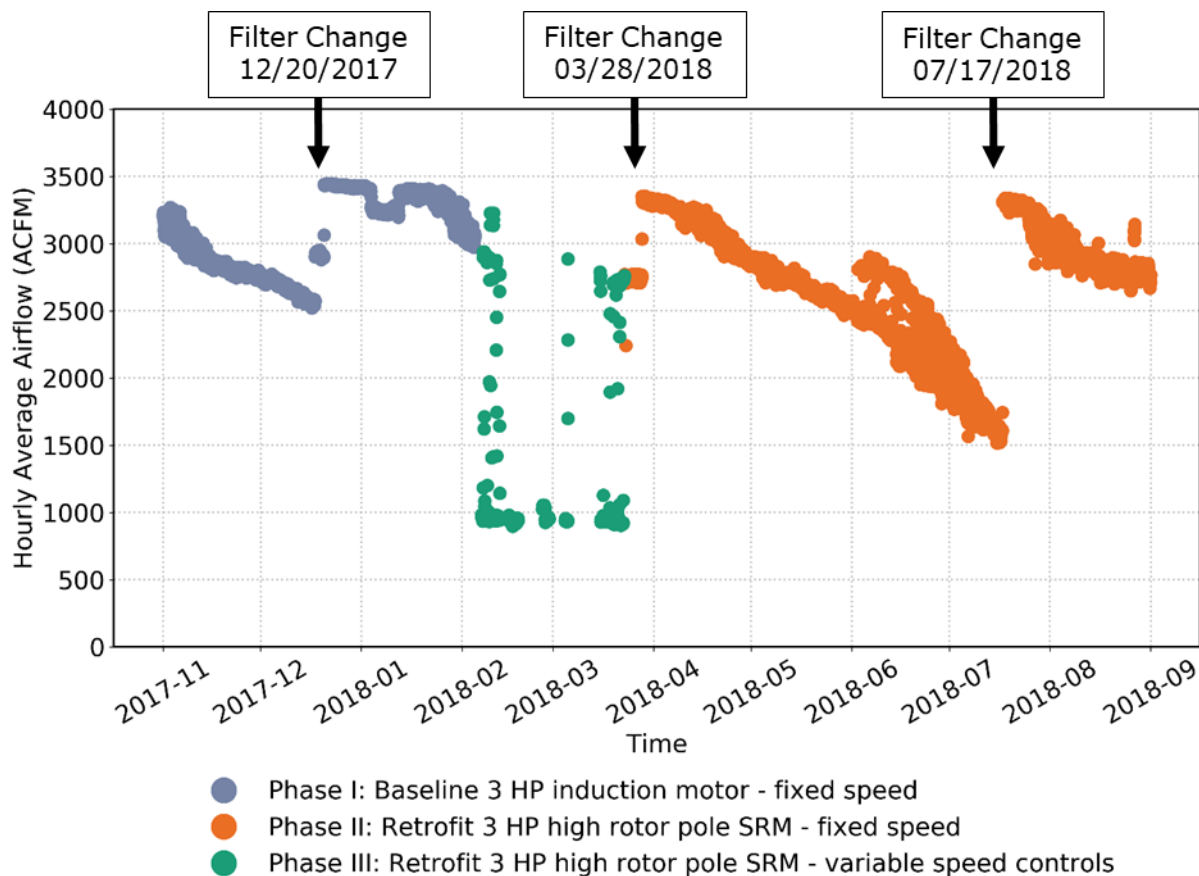


FIGURE 18: HOURLY AVERAGE AIRFLOW DURING FIELD TEST

Fan Power Intensity

Fan power intensity describes the amount of power (in watts) consumed per volume of air moved (in ACFM). A lower value indicates the fan system was operating more efficiently because it was able to move air using less power.

Figure 19 illustrates the hourly average fan power intensity of the baseline and high rotor pole SRM during the field testing period. As expected, the fan power intensity of both motors, while operating at a constant speed, increased as the airflow decreased, due to filter clogging. As filter clogging raised the airflow resistance, the power required to move the air also increased. Averaged over the field test, the high rotor pole SRM had a power intensity 11.2% lower at 1,725 RPM, and an even lower power intensity at lower fan speeds (Table 22).

Since filter clogging makes it difficult to directly compare two motors, their fixed-speed performance was also compared over a one-week time period, after filter changes. During the field test, three filter changes occurred: one with the baseline motor, and two with the high rotor pole SRM. No clean filter data was available for the high rotor pole SRM at reduced speed.

Figure 20 illustrates the hourly average fan power intensity of the baseline and high rotor pole SRM operating at 1725 RPM, as well as the best fit, which shows a small trend over the week. On average, the baseline and high rotor pole SRM had power intensities of 0.342 W/ACFM and 0.299 W/ACFM, respectively. The difference of 0.043W/ACFM represents a 12.3% decrease in power intensity for the high rotor pole SRM compared to the baseline.

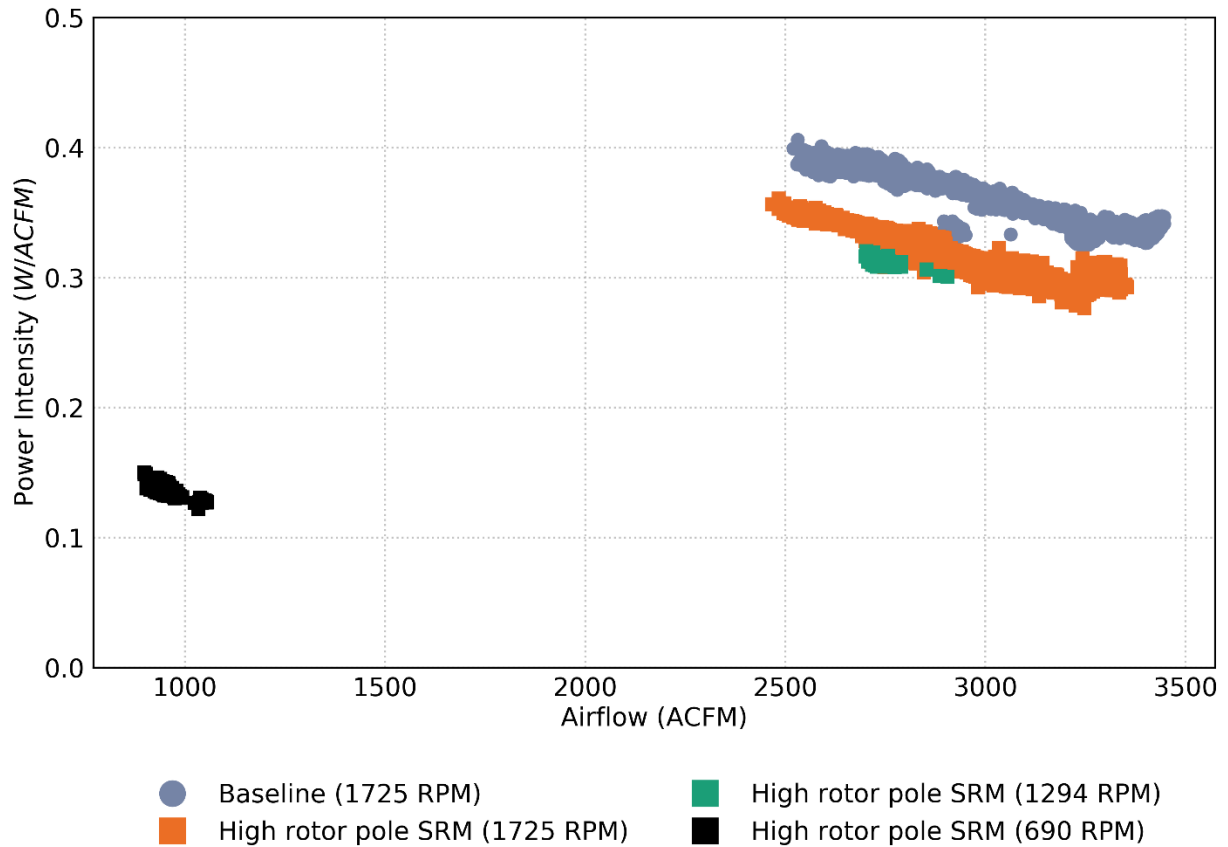


FIGURE 19: FIELD TEST FAN POWER INTENSITY COMPARISON

TABLE 22: AVERAGE FAN POWER INTENSITY RESULTS

	Field Test Average Power Intensity (W/ACFM)	After Filter Change Average Power Intensity (W/ACFM)
Baseline (1725 RPM)	0.357	0.342
High Rotor Pole SRM (1725 RPM)	0.317	0.299
High Rotor Pole SRM (1294 RPM)	0.313	-
High Rotor Pole SRM (690 RPM)	0.137	-

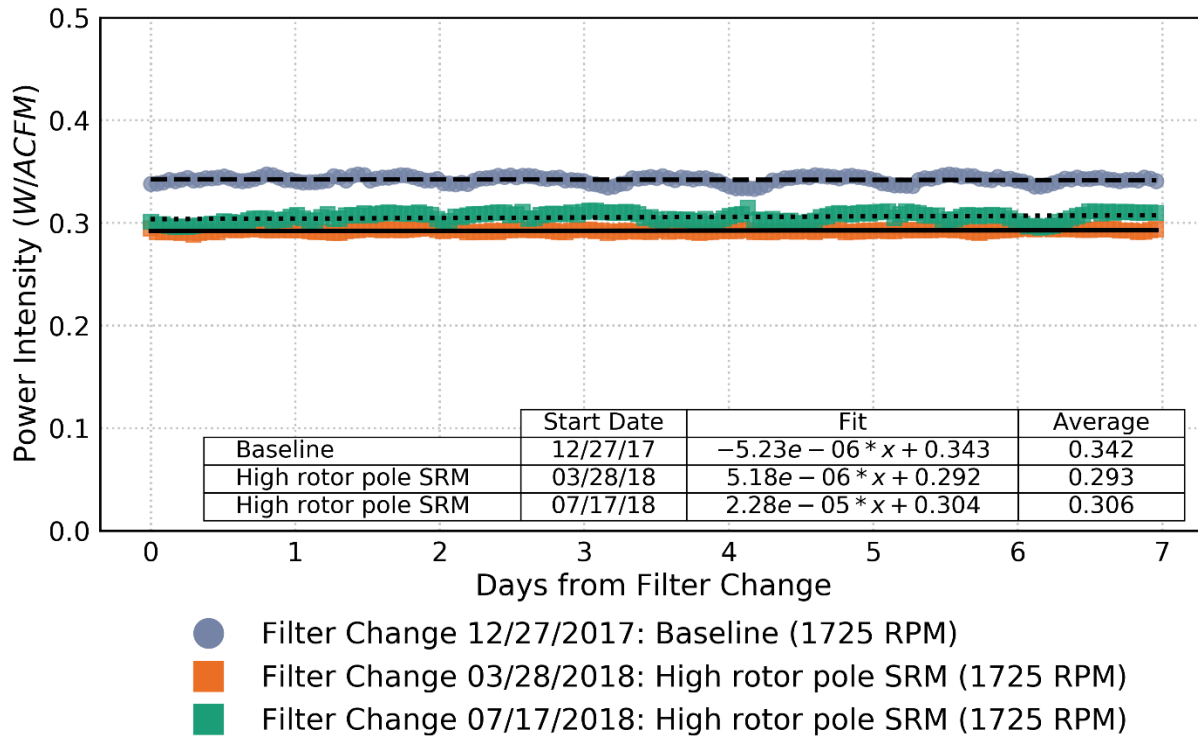


FIGURE 20: FIXED-SPEED FAN POWER INTENSITY COMPARISON

Airflow vs Power

Figure 21 illustrates the baseline and high rotor pole SRM’s hourly average power draw during the field test. Over the range of conditions, the baseline motor used 0.94 – 1.21 kW while operating at 1,725 RPM. At the same operating speed, the high rotor pole SRM used 0.837 – 1.083 kW. On average, the high rotor pole SRM reduced the required power draw by 15% compared to the baseline. With clean filters, power draw reduction increased to 15.7% (Table 23).

Operating at variable speed achieves additional savings by reducing the airflow rate, when full airflow is not required. During the variable speed portion of the field test, the high rotor pole SRM used 0.855 kW while operating at 1,294 RPM (75% of full speed) for Stage 1 cooling, and 0.131 kW while operating at 690 RPM (40% of full speed) for air circulation.

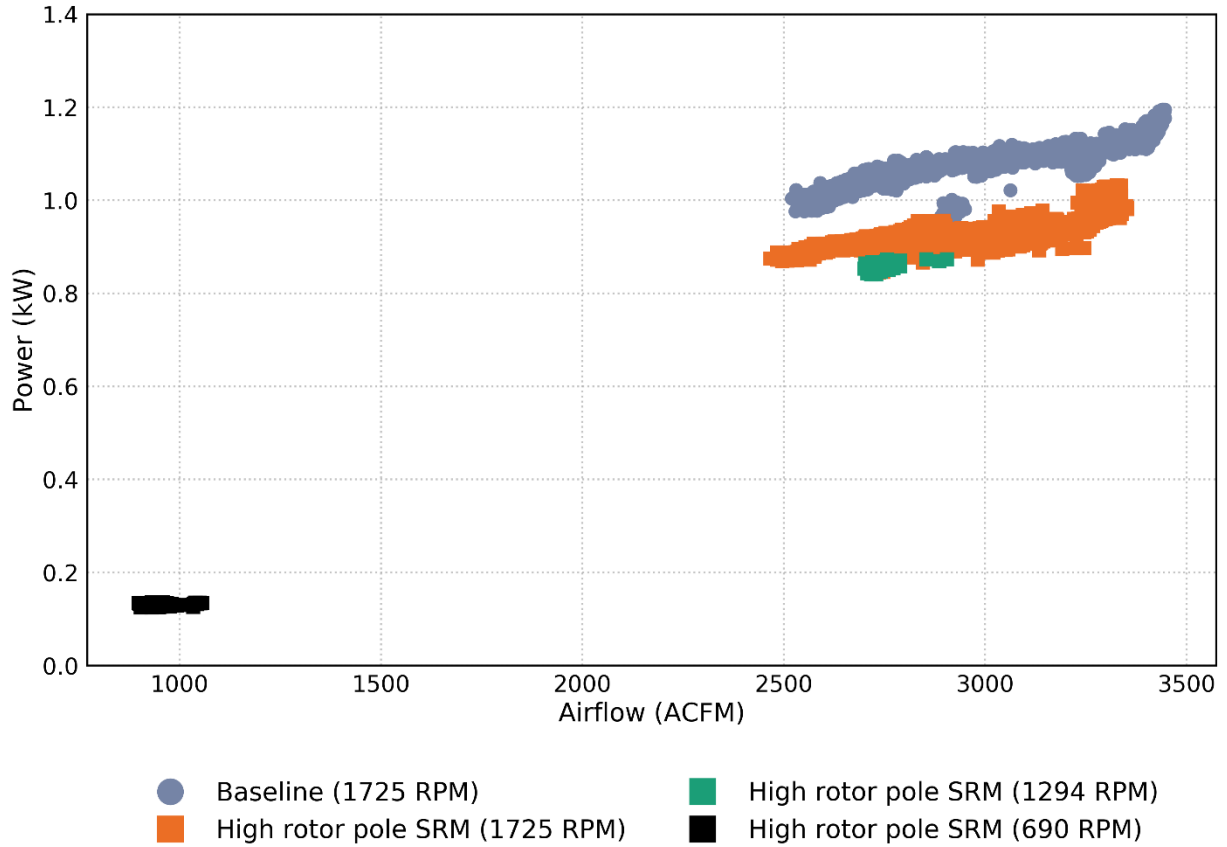


FIGURE 21: AIRFLOW VS. POWER

TABLE 23: AVERAGE POWER DURING FIELD TEST

	Field Test Average Power Draw (kW)	After Filter Change Average Power Draw (kW)
Baseline (1725 RPM)	1.089	1.174
High Rotor Pole SRM (1725 RPM)	0.926	0.990
High Rotor Pole SRM (1294 RPM)	0.855	-
High Rotor Pole SRM (690 RPM)	0.131	-

Uncertainty

The uncertainty for airflow, fan power, and fan power intensity are listed in Table 24. The uncertainty of the calculated metrics did not impact the field test results.

TABLE 24: UNCERTAINTY OF CALCULATED METRICS

Metric	Typical Value	Uncertainty
Airflow (ACFM)	2330	±17
Fan Power (kW)	1	±0.002
Fan Power Intensity (Watts/ACFM)	0.429	±0.0039

Summary – Field Testing

Based on field testing performance, the high rotor pole SRM is a promising method of reducing 10-ton RTU blower power energy use by 15%, when operating at a fixed speed. The high rotor pole SRM obtained these savings by operating with a fan power intensity that was, on average, 11.2% lower than the baseline induction motor. In addition to the general savings the motor achieved, the high rotor pole SRM could save additional energy by providing variable-speed operation to RTUs as a retrofit option.

Annualized Savings for SCE Service Territory

The 3HP high rotor pole SRM's potential annualized savings was calculated for a 10-ton RTU with a centrifugal indoor fan (15" in diameter and 15" deep) that conditioned a commercial space in SCE's service territory. Annual energy use for all three options was calculated using the results from the laboratory and field RTU testing (Table 25), the assumption the commercial space was open year-round for 14 hours per day with the RTU fan running, and the estimated number of hours annually (2371 hours) the RTU would operate in cooling or heating mode based on California End-Use Survey data [1].

For the laboratory RTU, each motor's total power draw was approximately double that of the same motor type installed in the field test RTU. This is because the laboratory RTU was operating with a significantly-higher total external pressure, which greatly impacted the motor's overall power draw and modeled annual kilowatt-hour (kWh) consumption.

The high rotor pole SRM's projected annual energy use was compared to a 3HP single-speed induction motor (Table 26, baseline) and a 3HP induction motor operating at variable speeds through VFD control (Table 26, option 1). Based on laboratory RTU testing, the high rotor pole SRM could reduce annual energy usage by 50% compared to the baseline single-speed induction motor, and 11% compared to an induction motor controlled by a VFD. The field test analysis showed the high rotor pole SRM could reduce energy usage by 57% compared to the baseline single-speed induction motor. The actual amount of energy saved in a particular application would depend on many factors, including fan size, total external pressure, ventilation schedule, and cooling/heating loads.

TABLE 25: INPUTS FOR SCE SERVICE TERRITORY ANNUALIZED ENERGY SAVINGS FORECAST

		Field Data ¹		Lab Data ²	
		Baseline Single-Speed Induction Motor	High Rotor Pole SRM	Baseline Induction Motor + VFD	High Rotor Pole SRM
Cooling/Heating	Airflow (ACFM)	3359	3222	3417	3511
	External Static Pressure (inWC)	0.459	0.394	0.308	0.315
	Dynamic Velocity Pressure (inWC)	0.047	0.043	0.375	0.391
	Total External Pressure (inWC)	0.505	0.437	0.683	0.705
	Power draw (W)	1174	990	2063	1899
Ventilation/ Air Circulation	Airflow (ACFM)	-	861	1477	1535
	External Static Pressure (inWC)	-	0.037	0.065	0.068
	Dynamic Velocity Pressure (inWC)	-	0.003	0.070	0.075
	Total External Pressure (inWC)	-	0.040	0.136	0.142
	Power draw (W)	-	131	335	244

¹Results were averaged over the one week field test periods with clean filters

²Results from Test 2 of laboratory RTU testing

TABLE 26: RESULTS OF SCE SERVICE TERRITORY ANNUALIZED ENERGY SAVINGS FORECAST

	Field Data Savings Results	Lab Data Savings Results
Baseline (single-speed induction motor) [annual kWh]	6428	10611 ¹
Option 1: Single-speed induction motor + VFD control [annual kWh]	-	5932
Option 2: High rotor pole SRM [annual kWh]	2754	5261
Percent savings option 1 over baseline	-	44%
Percent savings option 2 over baseline	57%	50%

¹Laboratory RTU baseline was calculated assuming the fixed speed fan would consume 125W less without the VFD controller

Conclusion

The high rotor pole SRM with software-controlled inverter is a promising option for reducing fan power in commercial RTUs, when compared to an equivalent-sized induction motor. In laboratory benchtop dynamometer testing, the high rotor pole SRM outperformed an induction motor and VFD system, using between 9.2-36.2% less power to produce the same torque at the same speed. In laboratory RTU testing, the high rotor pole SRM reduced fan power intensity to deliver the same ACFM by an average of 16.9%, 17.5%, and 21.3% for the low, medium, and high-airflow resistance conditions.

Field testing was conducted on a big box retail store in Corona, California, and results illustrated similar performance trends. On average, while operating at full speed, the high rotor pole SRM reduced power use by 15%, and operated at an 11.2%-lower power intensity. Additional savings was achieved when the high rotor pole SRM operated at variable speeds, when heating and cooling was not needed.

Based on the laboratory and field results, the high rotor pole SRM could reduce 10-ton commercial RTU fan energy in SCE's service territory by 50% to 57% when compared to a single-speed induction motor, and 11% when compared to a VFD-controlled induction motor.

Recommendations

Based on our study results, high rotor pole SRMs with software-controlled inverters show the potential to save energy and reduce demand in RTU indoor fan applications, when compared to equivalent-sized induction motors that operate at a single-speed or are controlled by a VFD. Within SCE's service territory, the high rotor pole SRM could reduce fan energy use by 50% to 57% when compared to the single-speed induction motor, or 11% when compared to a VFD-controlled induction motor. These savings were achieved through technological differences that allowed the high rotor pole SRM to operate at a higher efficiency over a range of load and speed conditions.

References

- [1] Itron, "California Commercial End-Use Survey," 2006.
- [2] Southern California Edison, "ET13SCE1030 Packaged Air Conditioning Unit Enhanced Controller", " Emerging Technologies Coordinating Council, 2014.
- [3] D. Studer, R. Romero, L. Herrmann and K. Benne, "Energy Implications of Retrofitting Retail Sector Rooftop Units with Stepped-Speed and Variable-Speed Functionality," National Renewable Energy Laboratory, Golden, CO, 2012.
- [4] P. Jacobs, V. Smith, C. Higgins and M. Brost, "Small Commercial Rooftops: Field Problems, Solutions and the Role of Manufacturers," in *National Conference on Building Commissioning*, 2003.
- [5] US Department of Energy Advanced Manufacturing Office, "Adjustable Speed Drive Part-Load Efficiency," US Department of Energy, Washington DC, 2012.
- [6] Ebray, B. Drury and A. Hughes, *Electric Motors and Drives Fundamentals, Types, and Applications*, Amsterdam: Elsevier, 2013.
- [7] R. Krishnan and J. Irwin, *Switched Reluctance Motor Drives*, Boca Raton: CRC Press, 2001.
- [8] P. C. Desai, M. Krishnamurthy, N. Schofield and A. Emadi, "Switched Reluctance Machines with Higher Rotor Poles than Stator Poles for Improved Output Torque Characteristics," in *Industrial Electronics Conference*, Porto, 2009.
- [9] M. Krishnamurthy and T. Creary, "Method for reliable control of high rotor pole switched reluctance machines". USA Patent US15016084, US15413007, US15800396 (pending), 04 02 2015.
- [10] Lennox, *SGA/SGB Series Unit Information*, Richardson, TX: Lennox Service Literature, 2010.
- [11] R. S. Figliola and D. E. Beasley, *Theory and Design for Mechanical Measurements*, 3rd ed., John Wiley & Sons, Inc, 2000.
- [12] ASTM International, "ASTM E2029-11. Standard Method for Volumetric and Mass Flow Rate Measurements in a Duct Using Tracer Gas Dilution," ASTM International, 2001.
- [13] U.S. Energy Information Administration, "Commercial Buildings Energy Consumption Survey," 2012.
- [14] ASHRAE, 111-2008 Measurement, Testing, Adjusting, and Balancing of building HVAC Systems.
- [15] J.-W. Ahn, *Switched Reluctance Motor*, Intech, 2011.
- [16] P. C. Desai and A. Emadi, "Switched Reluctance Machine". USA Patent US7230360, 12 6 2007.